Order Number 9009733

Ab initio calculations on imine-carboxyl complexes and neurotransmitters

Fugler-Domenico, Lillian M., Ph.D.

City University of New York, 1989

U·M·I
300 N. Zeeb Rd.
Ann Arbor, MI 48106

A

AB INITIO CALCULATIONS ON IMINE-CARBOXYL COMPLEXES AND NEUROTRANSMITTERS.

by

Lillian Fugler-Domenico

A dissertation submitted to the Graduate Faculty in Biochemistry in partial fulfillment of the requirements for the degree of Doctor of Philosophy, The City University of New York.

1989

This manuscript has been read and accepted for the Graduate Faculty in Biochemistry in satisfaction of the dissertation requirement for the degree of Doctor of Philosophy.

Sept 12, 1989
Date

Charlotte A. Russell
Chairman of Examining Committee

Sept. 12, 1989
Date

Executive Officer

Supervisory Committee

The City University of New York

Abstract

AB INITIO CALCULATIONS ON IMINE-CARBOXYL COMPLEXES AND NEUROTRANSMITTERS

by

Lillian Fugler-Domenico

Advisers: Professor C.S. Russell and Professor A.M. Sapse

Ab initio calculations are performed in order to investigate the methylene-imine complexes with formic acid using STO-3G and 6-31G basis sets. It is found, for the methylenimine-formic acid and N-methylmethylenimine-formic acid complexes, that (1) species found in the gas phase will exist as a neutral-neutral complex, (2) the STO-3G basis set is not adequate for the description of the charge-pair complex but predicts the correct trend in energy and (3) even though the allyl group stabilizes somewhat the charge-pair complex, the differences between the allylimine-carboxyl and methylenimine-carboxyl interaction are minimal.

Ab initio calculations are also used in order to determine the most stable conformations for γ-aminobutyric acid (GABA), GABA imine, aminooxyacetic acid (AOAA), taurine, hypotaurine and L-2,4-diaminobutyric acid (L-DABA). Structural characteristics are obtained and related to the abilities of the compounds to cross the blood-brain barrier (BBB). It is found that AOAA, which penetrates the BBB,

features an intramolecular hydrogen bond. GABA which does not cross the BBB, does not have an intramolecular hydrogen bond. Taurine, features an intramolecular hydrogen bond and has a lower proton affinity at the NH_2 group than GABA and therefore can penetrate the BBB, however slowly. GABA imine and hypotaurine which exhibited properties similar to GABA are predicted not to cross the BBB. The energies for the different conformations of L-DABA are so similar that it is postulated that L-DABA adopts a conformation complementary to a binding site due to its structural flexibility. The proton affinity predicts that L-DABA is a cation when GABA is a neutral molecule. This result correlates well with the experimental data, in that, in high-affinity transport, DABA requires one Na^+ while GABA requires two. As such, L-DABA is transported on the GABA carrier with a net charge of +2, where one charge is provided by the cotransported Na^+ and the second charge is contributed by the amino acid itself (L-DABA cation). Moreover, a similarity between the most stable cations of L-DABA (cycle) and GABA (partially-folded) are found and there is a possibility that the L-DABA cations are the species which may bind to the synaptosomal receptor.

Dedication

To my parents, Rita and Francois Fugler, who made many sacrifices through the years to help me achieve my goals in life.

To my husband Tom, for his patience and support.

Acknowledgements

To Dr. C.S. Russell and Dr. A.M. Sapse for their guidance, and determination to provide a well rounded scientific education.

To all other members of the scientific community that have aided in my development.

Table of Contents

List of Tables

List of Figures

Abbreviations

MINDO-3: modified intermediate neglect of differential overlap.

MNDO: modified neglect of differential overlap.

INDO: intermediate neglect of differential overlap.

SCF-MO: self-consistent field molecular orbital.

STO: Slater-type orbital.

AO: atomic orbital.

GABA: γ-aminobutyric acid.

AOAA: aminooxyacetic acid.

L-DABA: L-2,4-diaminobutyric acid.

Chapter 1. *Ab initio* calculations on imine-carboxyl complexes.

INTRODUCTION

A. *Ab initio* calculations.

Molecular conformations have been studied using theoretical quantum mechanical techniques such as semiempirical calculations, ie. MINDO-3, MNDO and INDO, and the more vigorous approach, *ab initio* calculations, which do not make use of empirical parameters. *Ab initio* calculations can provide useful information about bond lengths, bond angles, dipole moments and energies of different conformations of a given compound.

Ab initio calculations are iterative procedures which are based on self-consistent field-molecular orbital methods (SCF-MO). Calculations are approached by the Hartree-Fock (SCF-MO) method closed-shell approximation which treat a single electron at a time interacting with an aggregate of all the other electrons. The potential energy term, $V(r_i)$, of the Hamiltonian is expressed using the electron density which in turn is calculated via the initial guess for the wave function.

$$\left[\frac{-\hbar^2}{2m}\nabla_i^2 + V(r_i)\right]\psi_i(i) = \varepsilon_i\psi_i(i)$$

Solving the Schrodinger equation, a new set of eigenfunctions and energies are obtained. The new wave functions replace the preceding ones in the potential and a new equation is thus obtained. Self-consistency is

achieved when the difference in the energies obtained falls below a certain established threshold.

The ab initio calculations at Hartree-Fock level solve the Hartree-Fock equations which, for a closed-shell system take the form:

$$\hat{h}^F \psi_i(r) = \varepsilon_i \psi_i(r)$$

where $\hat{h}^F$ is the Hartree-Fock operator, ψ_i is the wave-function and the eigenvalues ε_i are referred to as the "orbital energies" and r labels the coordinates of the electron relative to the nucleus. The equations are solved iteratively until desired convergence is obtained. A full theoretical treatment of a polyatomic molecule, including geometry optimization, involves calculations for the electronic wavefunction for a range of bond lengths, bond angles and dihedral angles. A new set of parameters is obtained by setting the first derivatives of the energy to zero and calculating the matrix of the second derivatives. The procedure is repeated until the minimum in energy is obtained. The wave functions obtained are used to calculate the net atomic charges via Mulliken population analysis. Orbital energies and coefficients of atomic orbitals in different molecular orbitals are obtained.

Basis sets are used to describe the orbitals in a molecule. Pairs of electrons are assigned to molecular orbitals (ψ_i) which can be written as: $\psi_i = \sum c_i \chi_i$

where c_i is the coefficient given for each orbital and x_i is the basis function to describe each orbital. To facilitate the integrals calculations, the basis set used can be of Gaussian form. The Gaussian function can be written as: $\chi_i = exp(-\alpha r^2)$ where exp is the exponential function, α is the orbital exponent and r is the radial distance from the nucleus. The Slater orbitals are expanded thus in a series of Gaussians. The basis sets used are STO-3G, 3-21G, 6-31G and 6-31G* (1,2). The STO-3G basis set expands the Slater orbitals of the atoms in a series of three Gaussians and uses only one of each Slater orbital. The 3-21G basis set has three Gaussian-type orbitals per inner shell STO plus valence shell AOs split into two Gaussian inner and one Gaussian outer part. The 6-31G set uses one Slater orbital expanded into 6 Gaussians for the core electrons and the valence electrons use two Slater orbitals, an inner one expanded in 3 Gaussians and an outer one represented by 1 Gaussian. The 6-31G* is constructed by the addition of a singlet set of Gaussian d functions to the split valence 6-31G basis set.

The model systems in this project are all optimized by allowing all the molecular parameters to relax, thus yielding low energy (stable) species.

B. Importance of Schiff bases in biochemistry.

The aldimine or Schiff base moiety ($-\overset{H}{\underset{|}{C}}=N$) appears in the prosthetic groups of many proteins and has been impli-

cated in the mechanism of many enzymatic reactions. Pyridoxal phosphate (a derivative of vitamin B6) acts as a coenzyme in transamination reactions by forming covalent Schiff base intermediates with substrates. Aspartate transaminase, glutamate decarboxylase and GABA transaminase [the latter two enzymes are involved in the synthesis and degradation of the inhibitory neurotransmitter gamma-aminobutyric acid (GABA)] are examples of enzymes that involve Schiff base intermediates (3,4). In addition, other enzymatic mechanisms, such as those for acetoacetate decarboxylase, L-2-keto-3-deoxy-arabonate dehydratase and δ-amino-levulinic acid dehydratase require an imine linkage between substrate and a lysine residue of the enzyme (5-7).

Rhodopsin, the visual pigment in the disk membranes of vertebrate retinal rod cells,is composed of the chromophore, 11-cis-retinal, linked by a Schiff base to the membrane glycoprotein opsin. Many studies have confirmed by electronic spectroscopy that the chromophore is attached to the protein by a protonated Schiff base linkage in rhodopsin (8-11).

Retinal has an absorption maximum at 380 nm. However, when bound to opsin to form the visual pigment (rhodopsin), the absorption maximum shifts to the visible range, generally between 480 nm and 560 nm, depending on the animal species involved (12-14).

To explain this, Honig and coworkers (15,16) proposed

the "external point-charge model", which suggested that color regulation in visual pigments was achieved through chromophore-protein electrostatic interactions.

Figure 1

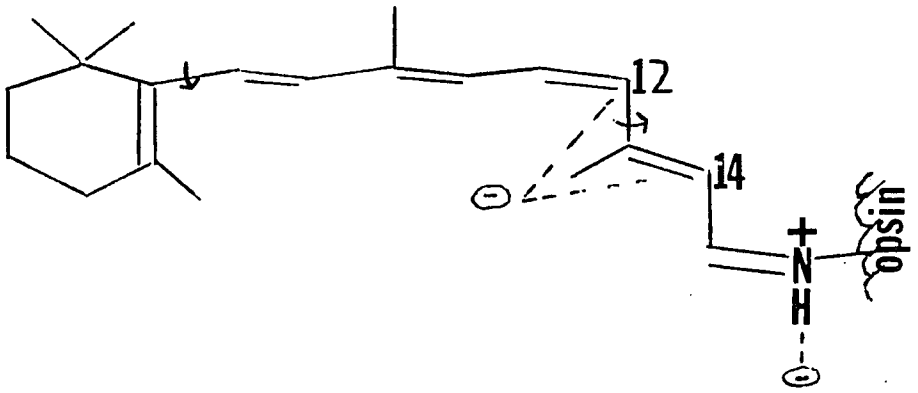

The external point-charge model showing the electrostatic interactions in the binding of bovine rhodopsin. A counter-ion is located near the protonated Schiff base linkage. A second negative charge is located 3 Å above C-12 and C-14. The arrows indicate that the bonds are twisted (16).

In this model (shown in Figure 1), Honig and coworkers proposed that the bathochromic shift was due to the electrostatic interactions between the protonated chromophore and a charged group located on the protein near carbon 12 and 14.

Bacteriorhodopsin (BR), found in the purple membrane of L. Halobacterium halobium, contains the chromophore, all-trans-retinal linked by a Schiff base to the terminal amino group of a lysine residue Figure 2 (17,18). It is

widely accepted that protonation of the Schiff base linkage is an essential component in the proton pumping activity of BR (17,18). Light absorption by the covalently-attached retinal chromophore results in a photochemical reaction cycle that is coupled to the translocation of protons across the bacterial cell membrane (19). BR converts light energy into the energy necessary to provide a hydrogen ion gradient that chemiosmotically drives the synthesis of ATP.

An "external point-charge" model was also developed for BR to explain the color and absorption maxima of the purple membrane (16). In this model, Nakanishi proposed that the electrostatic interactions between the protonated chromophore and a charge near the β-ionone ring was responsible for the opsin shifts of natural BR; namely, the origin of the color of the purple membrane (16).

Figure 2

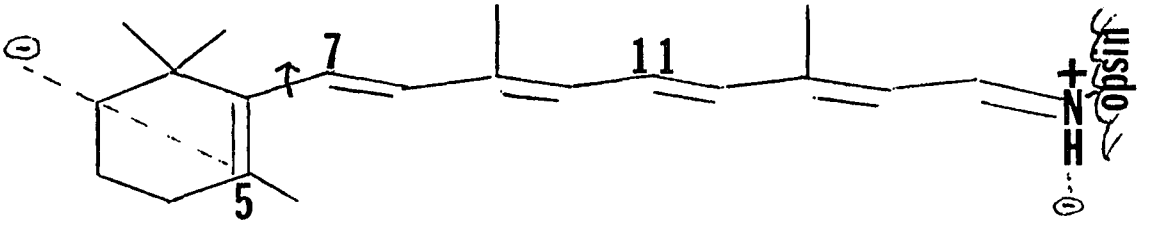

The external point-charge model showing the electrostatic interactions in the binding of BR. A negative charge is located near the protonated Schiff base. A second negative charge is located 3.5 Å above C5. The arrow indicates that the bond is twisted (16).

C. Theoretical studies on imine carboxyl interactions.

Since a protonated Schiff base was involved in the photocycle of rhodopsin and bacteriorhodopsin and an intermediate in several enzymatic reactions, it was of interest to try to describe the properties and geometries of the protonated Schiff base, especially in the presence of the carboxylate group which was its most probable counter-ion in a protein. Ab initio calculations have been used in order to understand model systems for the protonated Schiff base retinal chromophore in rhodopsin and bacteriorhodopsin. There was much controversy on the nature of the group donating a proton to the nitrogen in the Schiff base either by full protonation or hydrogen bonding. Studies using theoretical calculations have proposed that a carboxyl or an ammonium group was the potential proton donor to the nitrogen (20-22).

Hodošček and Hadži performed ab initio calculations using STO-3G and 4-31G basis sets with and without the inclusion of a perturbing charge for the retinal Schiff base-formic acid complex and allylimine-formic acid complex (23). The results at the STO-3G level showed that the neutral complex rather than the zwitterion was the dominant species, when a negative charge was added near the hydrogen bond. Using the 4-31G basis set, without inclusion of a negative charge, the results showed the neutral complex to be favored as the dominant species.

However, the inclusion of a negative charge near the hydrogen bond resulted in a lower energy for the zwitterion. The problem with this study was that calculations were performed without full optimization, which it will be shown latter to be necessary for the description of the system.

D. Description of thesis research.

This project involves the use of ab initio calculations to study imine-carboxyl interactions in the gas phase. The charge-pair complex and the neutral-neutral complexes for methylenimine-formic acid, N-methylmethylenimine-formic acid and N-methylallylimine-formic acid (studied in order to assess its effect on complexation energetics) are investigated in order to determine (1) the most stable molecular form and its conformation and (2) the proton transfer energetics. Also investigated is the double hydrogen-bonded neutral-neutral complex. This complex is studied because it had been shown that a carboxyl ion can form a double hydrogen bond with the guanidinium ion and therefore it seemed appropriate to investigate the possibility of the formation of a double hydrogen bond in this system also (24-26). The complexes investigated are the following:

(1) the single hydrogen bond neutral-neutral complex formed by the complexation of methylenimine with formic acid (Figure 3); (2) the single hydrogen bond charge-pair complex formed by the complexation of methyleniminium ion

with the formate ion (Figure 4); (3) the double hydrogen bond neutral-neutral complex (Figure 5); (4) the neutral-neutral complex formed by N-methylmethylenimine and formic acid (Figure 6); (5) the charge-pair complex formed by the complexation of N-methylmethyleniminium ion and formate ion (Figure 7); (6) N-methylallylimine-formic acid (Figure 8).

3

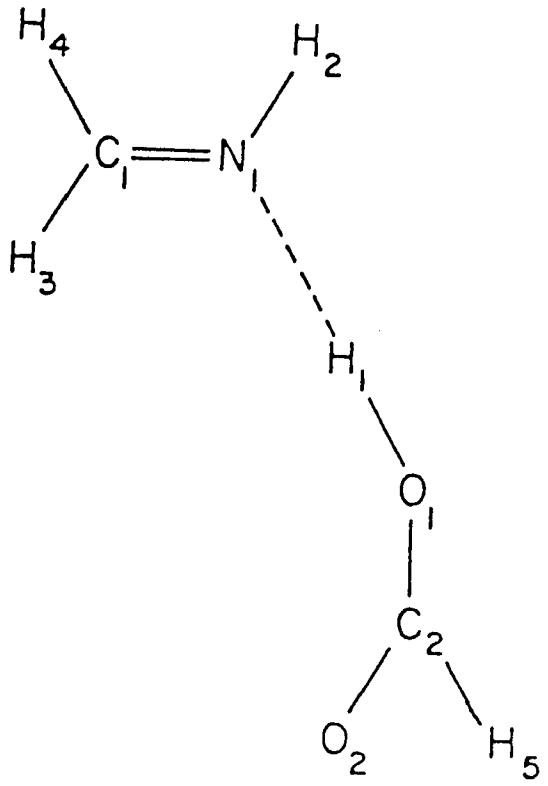

The single hydrogen bond neutral-neutral complex formed by the complexation of methylenimine with formic.

4

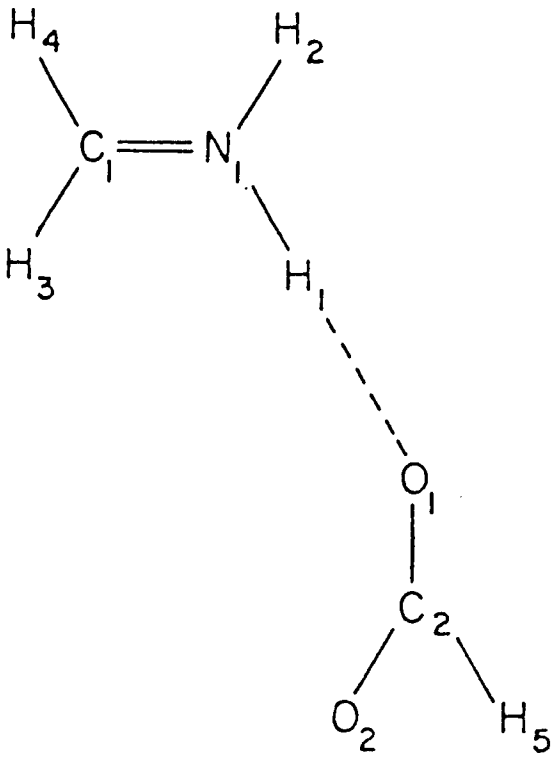

The single hydrogen bond charge-pair complex formed by the complexation of methyleniminium with formate.

5

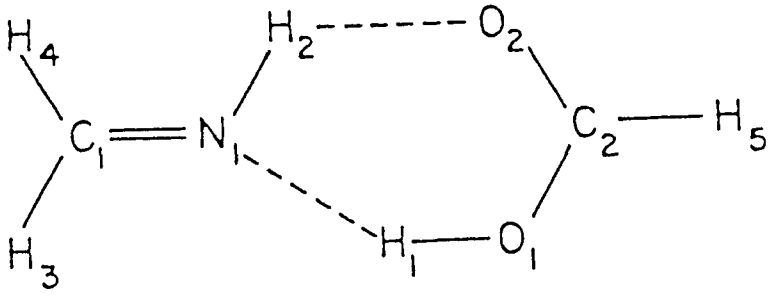

The double hydrogen bond neutral-neutral complex of methylenimine and formic acid.

6

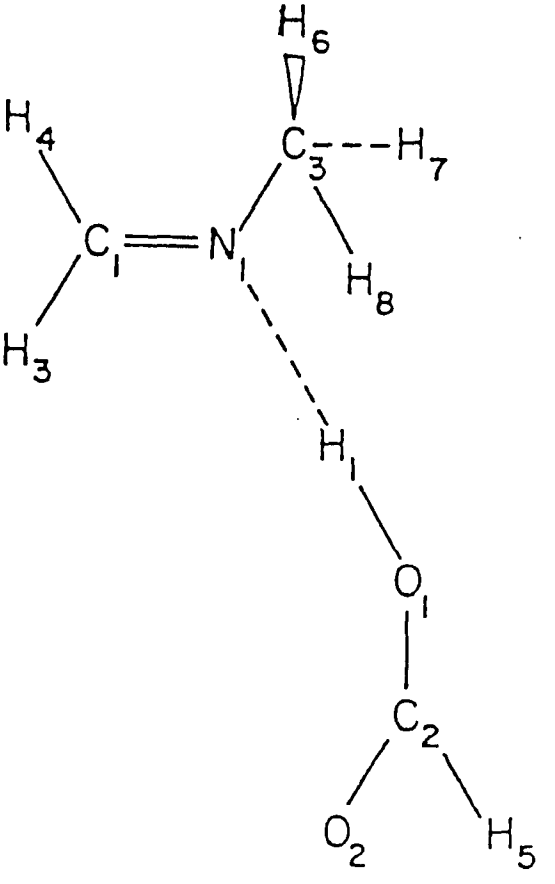

The neutral-neutral complex formed by N-methylmethylenimine and formic acid.

7

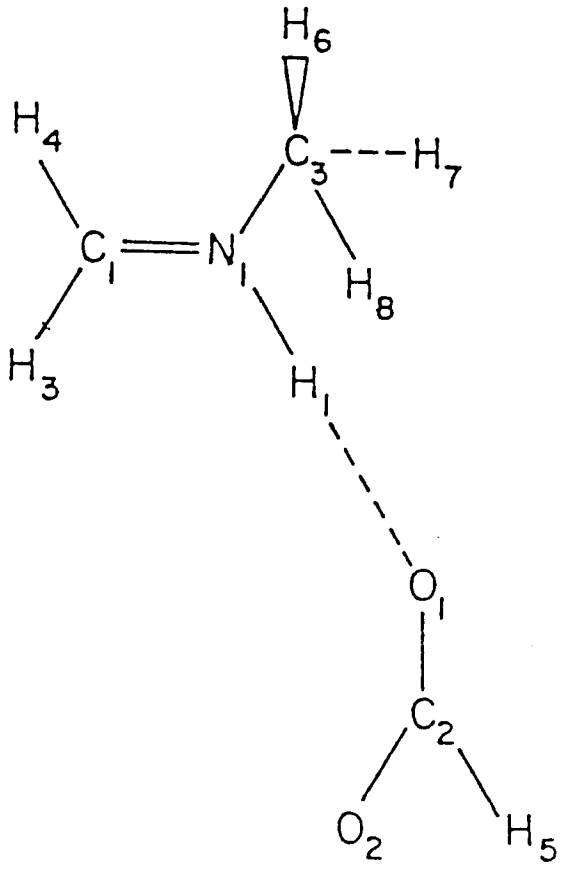

The charge-pair complex formed by the complexation of N-methylmethyleniminium and formate.

8

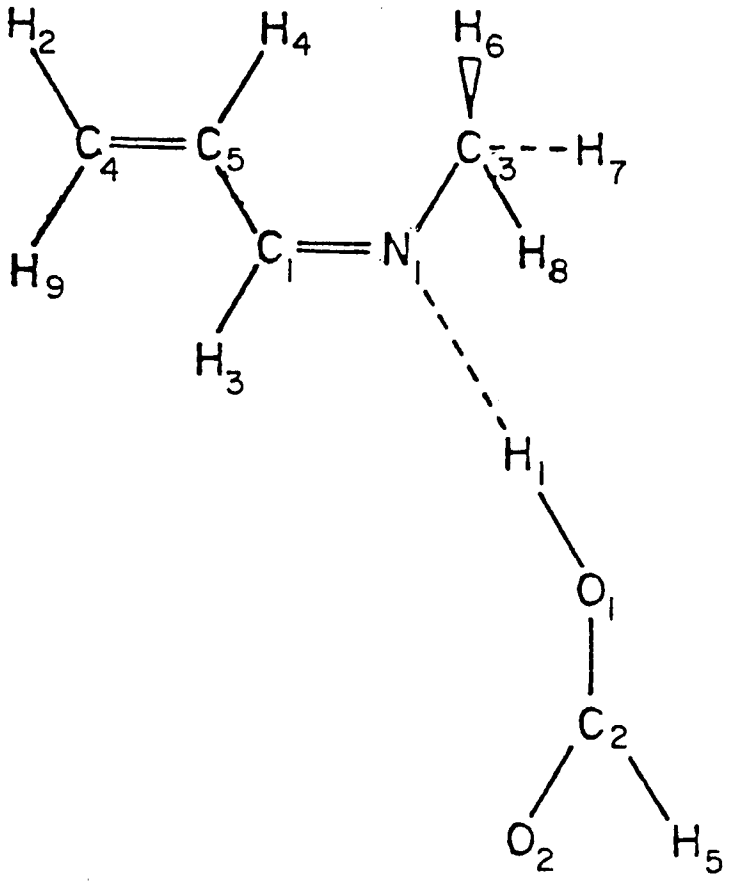

N-methylallylimine-formic acid.

METHODS

The method of calculation is the ab initio self-consistent field (Hartree-Fock) method using Gaussian basis sets as implemented by the Gaussian-80-computer program (27). The basis sets used are STO-3G and 6-31G (1,2). Each system is geometry-optimized by allowing all the molecule parameters to relax and using the Berny optimization technique (28).

The calculations on the N-methylallylimine-formic acid complex are performed for four N1H1 distances. N1H1 distances are kept frozen at 1.7 Å, 1.4 Å, 1.2 Å, and 1.03 Å while the other parameters are optimized.

The subsystems in this study (1) methylenimine, (2) methyleniminium, (3) N-methylmethylenimine, (4) N-methylmethyleniminium and (5) N-methylallylimine are all geometry-optimized with STO-3G and 6-31G basis sets. The formic acid and formate ion parameters are completely optimized with the STO-3G basis sets. The 6-31G basis set results for the formic acid and formate ion are taken from another study (24). The systems are set planar except for the N-methyl group in N-methylmethylenimine. The single hydrogen bond neutral-neutral complex formed by the complexation of methylenimine with formic acid is optimized subject to the following constraints: the angle formed by the plane of the imine and the plane of the formic acid, α, is set at three different values, $\alpha = 0^{\circ}$, 45°

and 90°, where the α=0° condition sets O2 cis to H3. For each of these, the rest of the parameters are optimized with the exception of N1H1O1 which is kept linear. The N1H1 bond length is set at the initial value of 1.02 Å and the O1H1 distance at 1.6 Å and allowed to optimize.

To calculate the lowest possible energy for the charge-pair complex, the N1H1 bond length is frozen at 1.03 Å and all the other parameters are optimized. α is kept at 0°.

The double hydrogen bond complex (formed by the complexation of methylenimine with formic acid, Figure 5) is allowed to relax its geometry through full optimization subject to the planarity constraints.

The N-methylmethylenimine-formic acid complexes are geometry-optimized subject to the following constraints (1) the angle formed by the plane of the imine and the plane of the formic acid, α, is set at two different values, 0° and 90°, (2) the rest of the parameters are optimized except for the N1H1O1 bond, which is kept linear. The charge-pair complex is also geometry-optimized while the N1H1 bond is kept at 1.03 Å.

The proton transfer for the single hydrogen bond complex (Figure 4) at 6-31G level of calculation is studied in the following way: the N1H1 distance is kept frozen at 1.2, 1.3, 1.4 and 1.5 Å. The rest of the parameters in the complex are optimized subject to planarity and to the linearity of the H-bond constraints. The binding energies of

the complexes are calculated by subtracting the energies of the separate systems from the energy of the complexes according to the following formula:

$$E_{binding} = E_{complex} - [E_{imine} + E_{HCOOH}]$$

RESULTS

Table 1 displays the energies and geometric parameters for the different subsystems using STO-3G and 6-31G calculations. Table 2 displays the energies and geometric parameters for the single hydrogen bond neutral-neutral complex formed by the complexation of methylenimine with formic acid (Figure 3) and the single hydrogen bond charge-pair complex formed by the complexation of methyleniminium ion with the formate ion (Figure 4) using 6-31G basis set (where N1H1=1.03 Å). Table 3 shows the energies and geometric parameters of the neutral-neutral complex formed by the complexation of N-methylmethylenimine and formic acid (Figure 6) and the charge-pair complex formed by the complexation of N-methylmethyleniminium ion and formate ion. (Figure 7) using STO-3G and 6-31G basis sets. Table 4 displays the proton affinities of the subsystems at 6-31G level of calculation. The proton transfer for the single hydrogen bond charge-pair complex formed by the complexation of methyleniminium ion with the formate ion is shown in Table 5. The binding energies using STO-3G and 6-31G basis sets for the single hydrogen bond neutral-neutral complex formed by the complexation of methylenimine with formic acid (Figure 3), the single hydrogen bond charge-pair complex formed by the complexation of methyleniminium with formate ion (Figure 4), the neutral-neutral complex formed by N-methylmethylenimine and formic acid (Figure 6)

and the charge-pair complex formed by the complexation of N-methymethyleniminium ion and formate ion (Figure 7) are shown in Table 6.

Table 1

Energies (au) and geometrical parameters (bond lengths in Å and angles in degrees) of methylenimine, methyleniminium, N-methylmethylenimine, N-methylmethyleniminium, formic acid and formate.

	$H_2C=NH$		$[H_2C=NH_2]^+$	
	STO-3G	6-31G	STO-3G	6-31G
E=	-92.8230	-93.9814	-93.2349	-94.3476
Bond lengths				
C1N1	1.273	1.261	1.292	1.271
C1H3	1.090	1.077	1.103	1.072
C1H4	1.090	1.077	1.103	1.072
C2N1	--	--	--	--
N1H1	--	--	1.038	1.002
N1H2	1.048	1.007	1.038	1.002
Bond angles				
H1N1C1	--	--	120.1	120.2
H2N1C1	109.1	115.8	120.1	120.2
H3C1N1	125.4	124.7	121.8	122.2
H4C1N1	119.1	115.8	121.8	122.2
C2N1C1	--	--	--	--

	$H_2C=NCH_3$		$[H_2C=NHCH_3]^+$	
	STO-3G	6-31G	STO-3G	6-31G
E =	-131.4051	-132.9924	-131.8285	-133.3716
Bond lengths				
C1N1	1.272	1.258	1.290	1.269
C1H3	1.090	1.073	1.100	1.071
C1H4	1.088	1.083	1.100	1.072
C2N1	1.500	1.464	1.509	1.482
N1H1	--	--	1.039	1.004
N1H2	--	--	--	--
Bond angles				
H1N1C1	--	--	118.2	118.6
H2N1C1	--	--	--	--

H3C1N1	119.0	119.4	120.4	120.4
H4C1N1	125.2	124.0	120.0	120.4
C2N1C1	114.9	120.5	124.9	126.2

	HCOOH		$HCOO^-$	
	STO-3G	6-31G	STO-3G	6-31G
E =	-186.2179	-188.6655	-185.4563	-188.0952
Bond lengths				
C2O2	1.214	1.204	1.266	1.257
C2O1	1.386	1.345	1.266	1.257
O1H1	0.990	0.956	--	--
H5C2	1.104	1.073	1.152	1.111
Bond angles				
O1C2O1	123.6	124.4	130.4	130.1
H1O1C2	104.8	114.9	--	--
H5C2O2	126.0	126.0	114.8	115.0

Table 2

Energies (au) and geometrical parameters [bond lengths (Å) and angles (degrees)] for methylenimine-formic acid (Figure 3) and methyleniminium-formate complex (Figure 4) obtained through the use of the 6-31G basis set where N1H1 is frozen at 1.03 Å.

	3			4
	α =0.0°	α =45.0°	α =90.0°	α=0.0°
Energies	-282.6706	-282.6677	-282.6491	-282.6525
Bond lengths				
N1C1	1.264	1.262	1.261	1.267
N1H1	1.731	1.751	1.787	1.03
N1H2	1.004	1.005	1.005	0.997
C1H3	1.073	1.073	1.073	1.078
C1H4	1.078	1.078	1.078	1.073
O1H1	0.988	0.985	0.981	1.525
C2O1	1.323	1.327	1.329	1.276
C2O2	1.216	1.214	1.211	1.254
C2H5	1.077	1.076	1.076	1.084
N1O1	2.719	2.736	2.768	2.555
Bond angles				
C1N1H1	116.3	119.4	127.0	118.2
C1N1H2	117.5	117.2	116.5	123.0
H3C1N1	118.7	119.1	119.4	116.0
H4C1N1	123.6	123.7	123.5	121.4
H1O1C2	115.2	116.5	117.9	105.5
O1C2O2	124.9	125.1	125.6	124.7
O2C2H5	112.1	111.8	111.4	116.7

Table 3

Energies (au) and geometric parameters (bond lengths in Å and angles in degrees) for the neutral-neutral complex formed by the complexation of N-methylmethylenimine and formic acid (Figure 6) and the charge-pair complex formed by the complexation of N-methylmethyleniminium ion and formate ion (Figure 7) using 6-31G basis set, where N1H1 is frozen at 1.03 Å.

	6		7	
	STO-3G	6-31G	STO-3G	6-31G
E=	-317.6366	-321.6817	-317.5721	-321.6679
Bond lengths				
N1C1	1.272	1.261	1.291	1.265
N1C3	1.497	1.465	1.475	1.463
N1H1	1.762	1.718	1.03 (set)	1.03 (set)
C1H3	1.090	1.073	1.293	1.077
C1H4	1.092	1.081	1.107	1.074
H1O1	.999	.991	1.366	1.531
O1C2	1.368	1.323	1.278	1.279
O2C2	1.219	1.216	1.290	1.249
H5C2	1.106	1.075	1.115	1.085
C3H6	1.090	1.082	1.090	1.079
Bond angles				
C3N1C1	119.1	121.7	128.7	126.8
H1N1C1	116.4	114.7	106.5	116.2
H3C1N1	118.4	119.0	107.4	116.5
H4C1N1	124.6	123.7	114.7	121.1
H6C3N1	110.1	110.3	109.4	109.5
H1O1C2	106.2	125.0	103.1	107.6
O1C2O2	124.8	112.0	128.0	124.7
H5C2O1	110.9	115.8	114.8	116.0

Table 4

Proton affinities (kcal/mol)[a] of methylenimine, N-methylmethylenimine, allylimine and formate at 6-31G level of calculation.

Subsystem	Proton affinity	Subsystem	Proton affinity
$H_2C{=}NH$[b]	230.0	$H_2C{=}CHCH{=}NCH_3$[d]	250.0
$H_2C{=}NCH_3$[c]	237.9	$HCOO^-$[e]	357.9

[a] 1 atomic unit (au) is equal to 627.5 kcal/mol.

[b] Proton affinity (P.A.) = $E_{(H_2C{=}NH_2^+)} - E_{(H_2C{=}NH)}$

[c] P.A.= $E_{(H_2C{=}\overset{+}{N}HCH_3)} - E_{(H_2C{=}NCH_3)}$

[d] P.A.= $E_{(H_2C{=}CHCH{=}\overset{+}{N}HCH_3)} - E_{(H_2C{=}CHCH{=}NCH_3)}$

[e] P.A. = $E_{(HCOOH)} - E_{(HCOO^-)}$

Table 5

Energies (au) of the proton transfer of H1 from N1 to O1 for the methyleniminium-formate complex (Figure 4).

NH (Å)	STO-3G	6-31G
1.03	-278.9892	-282.6525
1.20	-279.0045	-282.6577
1.30	-279.0332	-282.6585
1.40	-279.0434	-282.6653
1.50	-279.0493	-282.6682
1.70	-279.0543	-282.6706

Table 6

Binding energies (kcal/mol) for methylenimine-formic acid (Figure 3), methyleniminium-formate (Figure 4), N-methylmethylenimine-formic acid (Figure 6), N-methyl-methyleniminium-formate (Figure 7) using STO-3G and 6-31G basis sets.

	STO-3G			
	3	4	6	7
α				
0.0°	8.4	--	8.6	--
45°	7.6	--	--	--
90°	7.0	--	--	--
	6-31G			
0.0°	14.9	3.5	14.9	6.3
45°	13.1	--	--	--
90°	11.8	--	--	--

$$E_{binding} = E_{complex} - [E_{imine} + E_{HCOOH}]$$

DISCUSSION

It is clear from Tables 2 and 3 that the neutral-neutral complexes [the single hydrogen bond neutral complex of methylenimine with formic acid (Figure 3) and of N-methylmethylenimine with formic acid (Figure 6)] are more stable than their respective charge-pair complexes (Figures 4 and 7). Using 6-31G calculations, the difference in binding energy between Figures 3 and 4 is 11.4 kcal/mol while Figures 6 and 7 differ by 8.7 kcal/mol.

The geometries of the subsystems (shown in Table 1) do not exhibit any unusual or surprising features. The STO-3G basis set generally predicts longer bond lengths than 3-21G or 6-31G. Our results are in agreement with Del Bene for the formic acid, using STO-3G (29). The angles predicted by STO-3G are quite similar to the other two basis sets results with the exception of the H1O1C2 angle which is much smaller. These results are also similar to the description of the anion provided by the 6-31G* calculation (24). The O1H1 bond is similar in length for both basis sets. The parameters of the subsystems do not show a significant difference upon complexation except for an elongation of the O1H1 bond in formic acid. The O1H1 bond in 6-31G is elongated from .96 Å to .98 Å. STO-3G predicted the O1H1 bond length to stay constant at about 1 Å upon complexation.

The neutral double hydrogen-bond complex shown in Fig-

ure 5 does not represent a minimum in energy. When optimization is attempted it reverts to the single hydrogen-bond neutral-neutral complex, featuring a linear N1H1O1 bond with O2 cis to H2. Figure 5 is less stable by .4 kcal/mol than Figure 3. This fact suggests that the positioning of O2 cis to H3 is more stable than to H2. The distance between O2 and H3 when they are cis is smaller than the distance between O2 and H2 when O2 is cis to H2.

In the charge-pair complex (Figure 4) the N1H1 bond is frozen at a typical NH bond length (1.03 Å), where the NH bond is involved in hydrogen bonding. The rest of the parameters in the complex are varied in order to obtain the lowest possible energy (within the constraints of planarity and keeping the N1H1O1 bond linear). The 6-31G results show that this structure has a minimum energy as long as the N1H1 bond is kept frozen at 1.03 Å. The STO-3G results differ in that a minimum could not be found even after an exhaustive search. A simple explanation is that the STO-3G basis set is not adequate for this system.

In Table 5, when the proton is transferred from the iminium to the formate, no minimum is found for the charged-pair complex at all calculated levels. This result contradicts the results of Hodošček and Hadži (23), who find a barrier to the proton transfer from the allyliminium to the formate. This difference can be explained by the fact that the double bond of the allyl group stabilizes

the charge-pair complex and produces a second minimum. An argument in favor of this explanation is the higher proton affinity of N-methylallylimine (250 kcal/mol) as compared to N-methylmethylenimine (237.9 kcal/mol), (see Table 4). However, this difference in proton affinity is too small to account for a large difference in the energetics of complexation. Another reason for the difference in proton affinities between this study and those of Hodošček and Hadži, is that in the latter study there was a lack of complete optimization in the geometric parameters. Moreover, when we repeated their calculation for the allylimine-formic complex, using the 6-31G basis set and optimizing the systems completely, a shallow minimum at N1H1=1.07 Å is found. The barrier found around N1H1=1.2 Å is very small (.25 kcal/mol) as opposed to 22 kcal/mol found by Hodošček and Hadži (23). These differences show that complete optimization is essential in these systems. It can be concluded that even though the allyl group stabilizes the charge-pair complex somewhat, it does not present a significant barrier to the proton transfer.

The binding energies shown in Table 6 are much larger for the 6-31G calculations than for the STO-3G. As mentioned before the STO-3G is not adequate for the description of the charged-pair complex.

When the angle α is varied in Figure 3, the highest binding energy is obtained for $\alpha=0^{\circ}$. The decrease

in energy with the increase in α is probably due to the fact that the electrostatic stabilization due to the proximity of O2 and H3 is removed. However there is substantial binding energy even for $\alpha=90^{\circ}$, since the O1H1 bond is not displaced. Consequently, in an environment where the imine and the carboxyl are set perpendicular to each other they will still hydrogen bond.

It can be concluded, for the methylenimine-formic acid complex and N-methylmethylenimine-formic acid complexes, that (1) species found in the gas phase will exist as the neutral-neutral complex, and (2) the STO-3G basis set is not adequate for the description of the charge-pair complex but predicts the correct trend in energy.

All the above calculations are performed for the gas phase. However in the methylamine-acetic acid complex it was shown that a polar solvent such as water stabilizes the charge-pair complex preferentially (30). Therefore, it is to be expected that solvation may alter these results substantially. The experimental study using ^{1}H NMR and UV spectroscopy for allylimine-formic acid in chloroform and in methanol support this expectation (31,32). It is shown by Bissonnette and coworkers that the acidic proton on a protonated Schiff base is very labile and exchanges rapidly between the imine group and solvating species (if the medium is polar) or the counterion, if it

is a carboxylate anion and the medium is non-polar.

Jain and coworkers studied the solvent effect on N-methylmethylenimine-formic acid and N-methylallylimine-formic acid complex using ab initio calculations (33). The purpose of this work was to investigate (1) a possible increase of the stabilities of the ion-pair complexes versus the neutral-neutral complex by the solvent and (2) to study the effect of the solvent on the complexation energies. The polar solvents favor the ion pair complex over the neutral complex, bringing them, in the case of water, within 1 kcal/mol of each other in their energy. As the solvent becomes less polar (ie. ether-furan-benzene-pentane), this effect diminishes.

Chapter 2. *Ab initio* calculations on GABA, GABA imine, AOAA and L-DABA.

INTRODUCTION

γ-aminobutyric acid (GABA) has been shown to be an inhibitory neurotransmitter in the mammalian central nervous system (34). It is present in cerebellar Golgi, basket and stellate cells, neostriatal spinal cord and cortical interneurons , nigrostriatal and pallidonigral neurons, and hippocampal basket cells (35-37).

GABA is formed in the brain (Figure 9) from glutamic acid by the action of the enzyme glutamic acid decarboxylase (GAD), a pyridoxal phosphate-dependent enzyme (38-40). GABA is metabolized by being converted to succinic semialdehyde (SSA) in nerve terminals and in glial cells. This conversion is mediated by GABA transaminase (GABA-T), a pyridoxal phosphate-requiring enzyme (38,41). The metabolic pathway for GABA is shown in Figure 9.

Figure 9

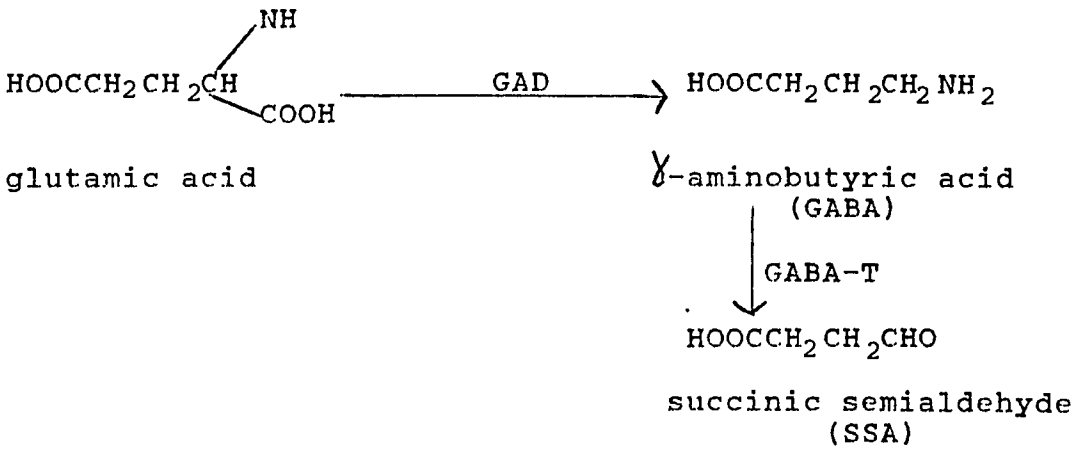

The transport processes, neuronal uptake and glial uptake of GABA are shown in Figure 10. These processes are largely responsible for the regulation of extracellular GABA levels and termination of synaptic transmission by GABA (4,42).

Figure 10

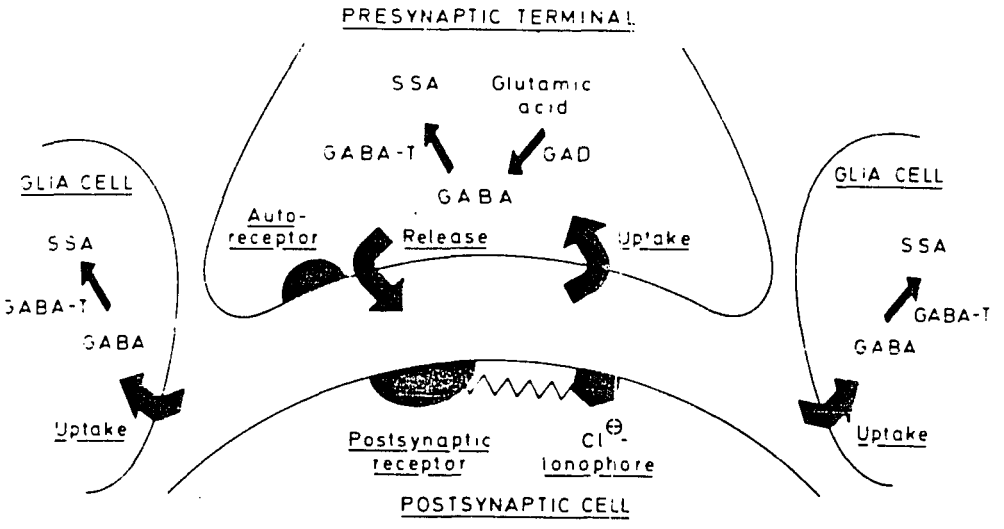

[Krogsgaard-Larsen, (4,42)]

Inactivation of synaptically released GABA is by neuronal and glial uptake transport processes. Inhibition of either neuronal or glial uptake leads to prolongation of the physiological effects of GABA. Thus some GABA analogues can act selectively on neuronal or glial uptake. L-2,4-diaminobutyric acid (L-DABA), 3-hydroxy-5-aminovaleric acid and cis-3-aminocyclohexane carboxylic acid (ACHC) are se-

lective inhibitors of neuronal GABA uptake, while β-alanine, β-proline, cis-4-OH nipecotic acid, homo-nipecotic acid, the bicyclic isoazoles, 4,5,6,7-tetrahydro-isoxazolo-[4,5 c]-pyridin-3-ol [THPO] and 5,6,7,8-tetra-hydro-4H-isoxazolo-[4,5 c]-azepin-3-ol [THAO], are all glial-selective GABA uptake inhibitors (43). It has been proposed that some model compounds such as L-DABA and β-alanine may be cell-type specific (44). Other functional aspects of neuronal and glial GABA uptake processes have been studied. It has been found that both neuronal and and glial uptake require two Na^+ for transport of GABA (45-48). GABA transport systems have been divided into two general classes: (1) the high-affinity transport systems (which are Na^+-dependent) and (2) the low affinity transport systems. The high-affinity Km values for GABA in mouse cell culture are 13-40 μM in cerebral astrocytes, and 5-11 μM in cortical neurons and 22-43 μM in rat cerebral cortex slices (49-52). High-affinity Km values varied from .5 to 100 μM with most values in the 10-40 μM range. The low affinity Km values are generally about 400 μM [ie. 400 μM in rat cerebellum slices, 500 μM in rat pons-medulla slices and 350-380 μM in rat cerebral cortex (52)].

It is evident from numerous biochemical, physiological and pharmacological studies that alterations in GABA neurotransmission may play a role in the pathology of epilepsy and seizures (4,42,43,53). Analysis of brain

samples from sites near seizure foci in epileptics and in animals made epileptic, reveal low levels of GAD (54-58). Moreover, it has been found that there is severe reduction of GAD activity and GABA content in the basal ganglia of patients with Huntington's chorea (59-61).

Direct administration of GABA, inhibition of reuptake processes and of GABA transaminase have all proved useful in the regulation of some types of epilepsy (62). GABA's inability to penetrate the blood-brain barrier (BBB) makes its direct use in the regulation of epilepsy and seizures impractical (4,42,62). However, alteration of GABA activity can be carried out by the use of GABA mimetics which are able to cross the BBB. Biomimetics of GABA can only function if they cross the BBB and after doing so can potentiate GABA action by binding in a similar way to receptors, by blocking degradation or by stimulating synthesis of GABA. Passage through the BBB is not a simple process, owing to the complex nature of what really is a "brain barrier system". Even if one accepts passage through the capillary endothelial cells as a rate-limiting step, many other anatomical features (i.e. the choroid plexuses, the arachnoid membrane, neuronal and glial transport processes, and inter-/intracellular metabolism) come into play before a substance can impact the inter- or intraneuronal environment (63). Aminooxyacetic acid (AOAA), [4,5,6,7-tetrahydro-isoxazolo(5,4-c)-pyridin-3-ol (THIP),

4-amino-5-fluoro-pentanoic acid, and 4-amino-hex-5-enoic acid (γ-vinyl GABA) are all potent inhibitors of GABA-T (4,42,64-66). Moreover, AOAA,THIP and γ-vinyl GABA are BBB-penetrable (64,66-68). γ-vinyl GABA has been shown to be a potent drug for the treatment of epilepsy (69). Yunger and his colleagues (62) have demonstrated useful anticonvulsant activity in two orally-active compounds, N-(4,4-diphenyl-3-butenyl)-nipecotic acid (SK&F 89976A) and N-(4,4-diphenyl-3-butenyl)-guvacine (SK&F 100200A), which are potent inhibitors of GABA transport (neuronal and glial uptake). Nipecotic acid and guvacine were found to be competitive inhibitors of high-affinity uptake in catfish whole brain (71). 4-(4-Azidobenzoimidylamino)-butanoic acid (ABBA), has been shown to be a potent inhibitor of synaptosomal GABA uptake (71). This may be attributed to the phenyl group in its structure which might make it BBB-penetrable (70). Further pharmacological studies on ABBA has not been reported in the literature. Muscimol, a fungal toxin, is the most potent and specific GABA agonist (4). It acts at the GABA receptor to mimic the physiological action of GABA. Muscimol can penetrate the BBB, however, it is rapidly decomposed after peripheral administration (4).

A structural analogue of GABA, L-2,4-diaminobutyric acid (L-DABA) which differs from GABA only by the presence of an additional amino group, has been shown to block

high-affinity neuronal uptake of GABA selectively (4,42, 72,73). It has been suggested that GABA and DABA may be transported by the same high-affinity protein carrier 74-76). It has also been suggested that DABA, unlike GABA can cross the BBB (77).

In vivo studies, on mice, which involved intraperitoneal and intracerebroventricular administration of DABA yielded results which suggested that DABA acts through several GABA related mechanisms (78). Meldrum and coworkers showed that DABA was a neuron-selective transport inhibitor which functioned as a convulsant or proconvulsant after intracerebroventricular injection (53).

Erecinska and coworkers (47) have shown that, in a synaptosomal fraction from rat brain, transport of GABA and DABA is mutually competitive [see also (70,79)]. pH studies showed that DABA is transported as a monovalent cation ($DABA^+$). In addition, it was shown that DABA is cotransported with one Na^+ and it was suggested that the protonated alpha-amino group on DABA is positioned near the second Na^+ site on this high-affinity carrier.

Structure studies can provide knowledge about the geometry, and charge distribution of molecules and the relation of these properties to the ability to penetrate the BBB. The PCILO and STO-3G ab initio calculations of Pullman and Berthod have indicated that the zwitterion of GABA is highly-folded (80). On the other hand,

the Huckel calculations of Kier and Truitt (81) have indicated that the best conformation is the extended one. These studies did not report data on the neutral species. Warner and Steward (82) studied GABA and its zwitterion using the CNDO/2 method (82). The results indicated that in the non-zwitterion form the preferred conformation was the partially-folded one. For the zwitterion, the results indicated that the partially-folded conformation was preferred also. However, they pointed out that the CNDO method was deficient in that it allowed too close contact between atoms. It also did not describe hydrogen bonds well.

The problem of relating structural characteristics of molecules to their ability to penetrate the BBB will be considered. It has been found that many lipid-soluble molecules such as nicotine, ethanol and heroin, can cross the BBB . While morphine does not cross the BBB, heroin, the diacetylated derivative of morphine can cross it because two highly polar -OH groups are replaced by $-O-\overset{O}{\overset{\|}{C}}-CH_3$ groups (83).

This work describes ab initio calculations, performed in order to elucidate the conformations and charge distributions of the neutral species of GABA, GABA imine, AOAA and L-DABA in the gas phase. . The gas phase may serve as a good model to mimic the non-hydrated environment of (1) the inner membrane leaflet, which must be traversed in

the course of crossing the BBB or (2) the hydrophobic receptor-binding site. The membrane is the barrier between the two aqueous compartments, the cytosol and extracellular medium. It is structurally composed of a polar lipid bilayer whose polar headgroups face the aqueous compartments and whose hydrocarbon side chains meet to form a hydrophobic lipophilic medium in the membrane.

Ab initio calculations can provide useful information on bond lengths, bond angles, dihedral angle, energies and molecular conformations that may exist in a particular model system. A comparison of the structural characteristics of GABA, GABA imine, AOAA and L-DABA is addressed in order to identify the similarities and differences between their lowest energy conformations. The ability of L-DABA to inhibit GABA, in high-affinity transport in synaptosomal tissue (79) is correlated with the conformational structures of L-DABA: extended, partially-folded and cyclic. The compounds studied are:

(1) γ-aminobutyric acid (Figure 11) in a partially-folded (a), in a cyclic, where H1 is hydrogen-bonded to N1, (b) and in an extended conformations (c);

(2) γ-aminobutyric acid imine (Figure 12) in a partially-folded (a) and a cyclic conformation (b);

(3) aminooxyacetic acid (Figure 13) in a partially-folded (a), a cyclic, where H1 is hydrogen-bonded to N1 (b) and another cyclic conformation where H1 is hydrogen-

bonded to oxygen (O1) (c);

(4) the cations and anions of GABA, GABA imine, and AOAA (see Methods);

(5) L-DABA (Figure 14) in an extended (a), in a partially-folded (b) and cyclic conformations (c);

(6) the cyclic cations of L-DABA (Figure 15a-c);

(7) cations of L-DABA extended and partially folded;

(8) anions of L-DABA in the extended, partially-folded, and cyclic conformations and L-DABA cyclic zwitterion.

The structure of GABA imine is studied because the reactions catalyzed by GABA transaminase and glutamate decarboxylase involve the initial formation of a Schiff base. It is of interest to study the structural properties of a model for this intermediate which may behave as an enzyme inhibitor for GABA-T thus increasing GABA levels at the synapse and to try to predict if it will cross the BBB. Experimental studies have shown that compounds which inhibit GABA-transaminase had considerable potential as anticonvulsant drugs (84).

L-DABA is examined in order to obtain information, which could provide insights into the similarities and differences in the transport behaviors of GABA and DABA.

11a

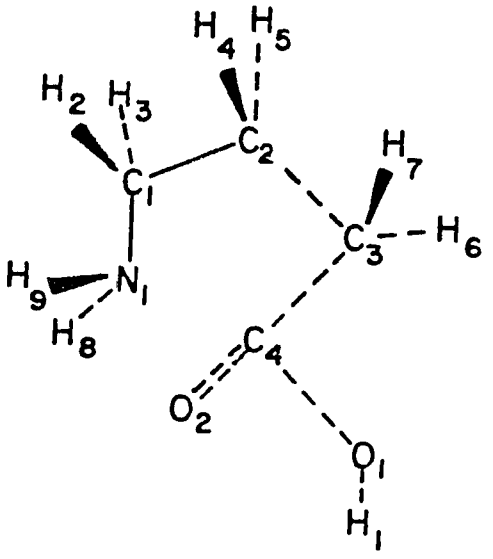

GABA in a partially-folded conformation.

11b

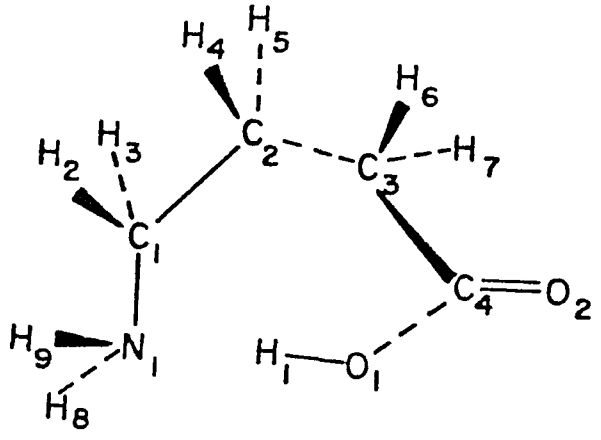

GABA in a cyclic conformation.

IIc

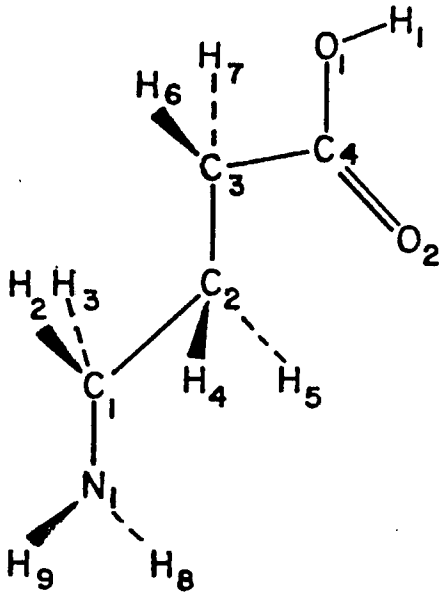

GABA in an extended conformation.

12a

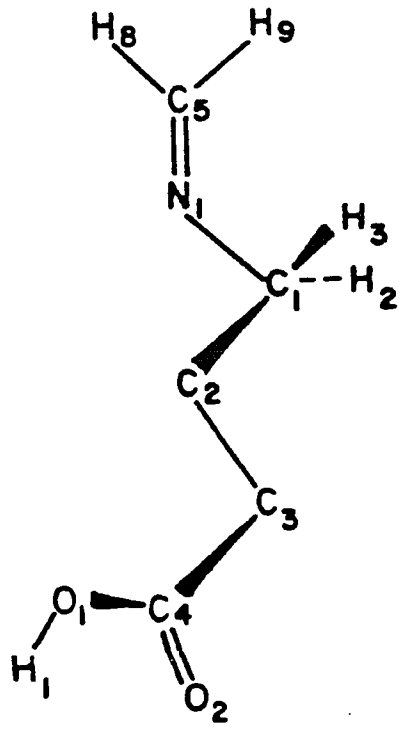

GABA imine in a partially-folded conformation.

12b

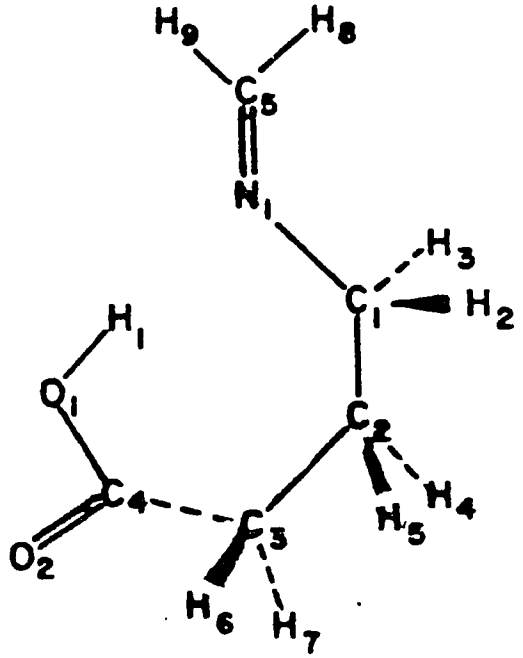

GABA imine in a cyclic conformation.

13a

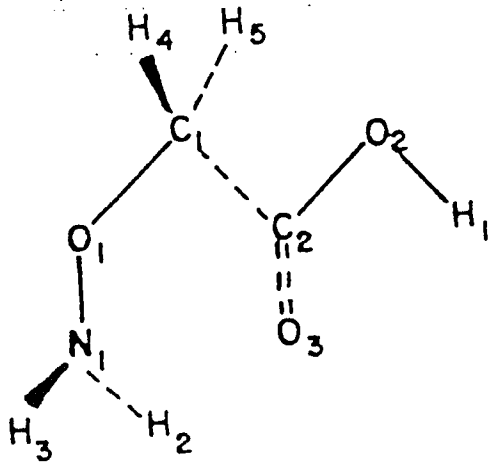

AOAA in a partially-folded conformation.

13b

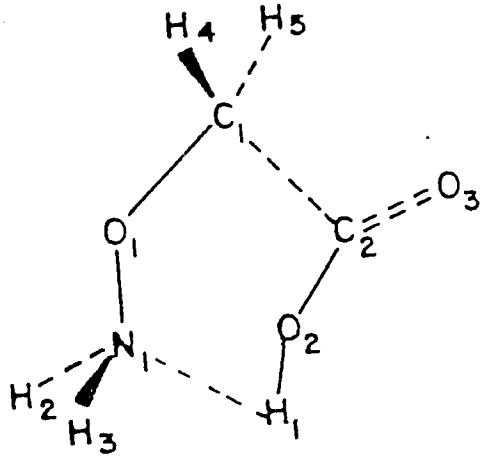

AOAA in a cyclic conformation, where
H1 is hydrogen-bonded to N1.

13c

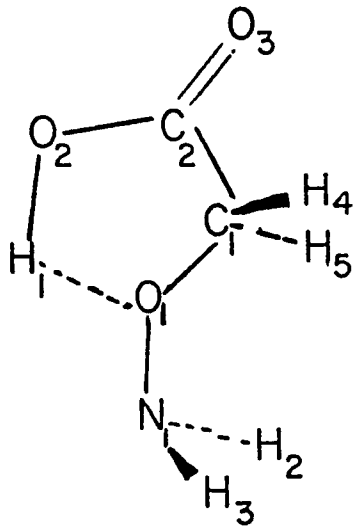

AOAA in a cyclic conformation, where H1 is hydrogen-bonded to O1.

14a

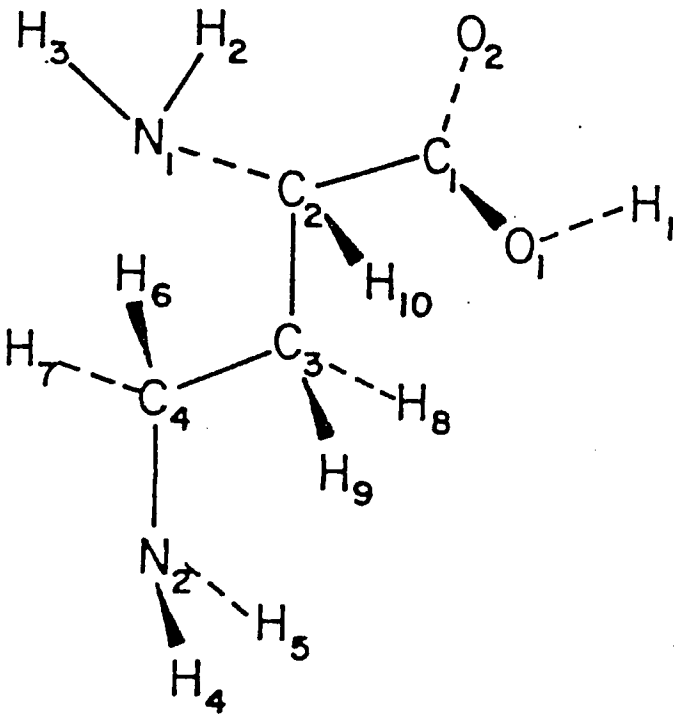

L-DABA in an extended conformation.

14 b

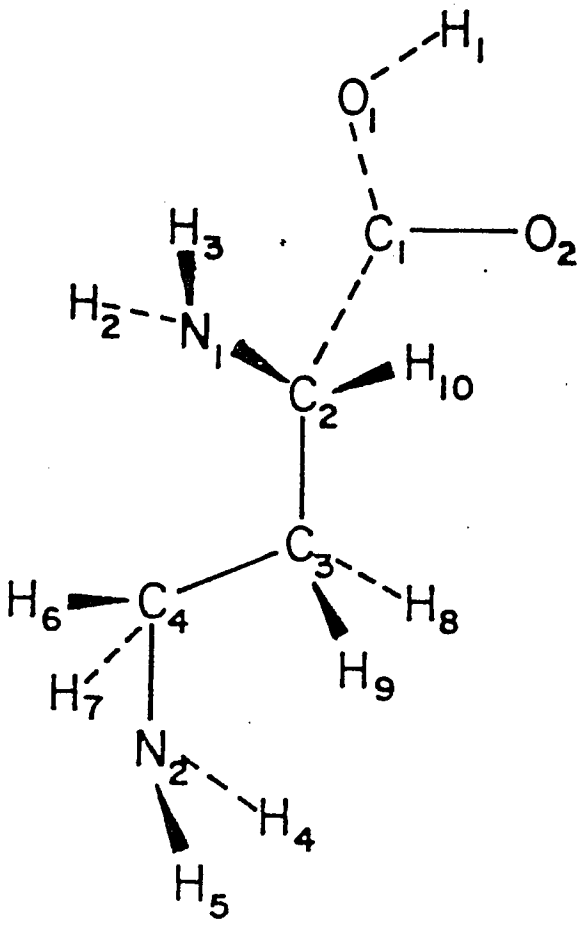

L-DABA in a partially-folded conformation.

14c

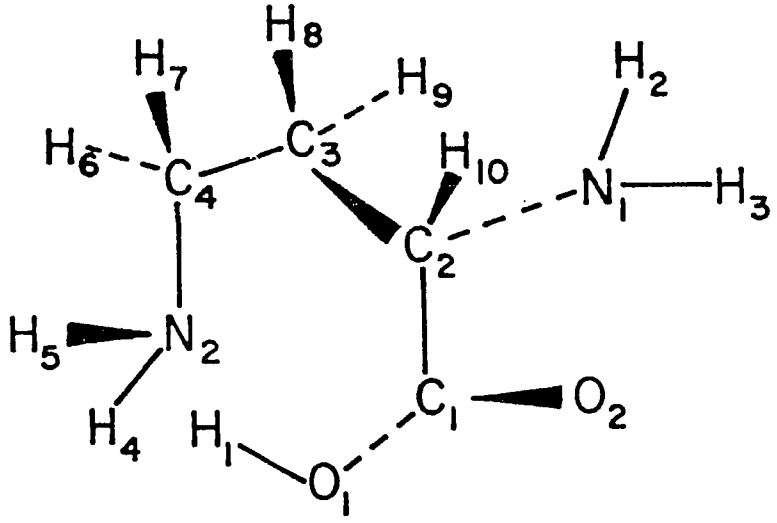

L-DABA in a cyclic conformation.

15a

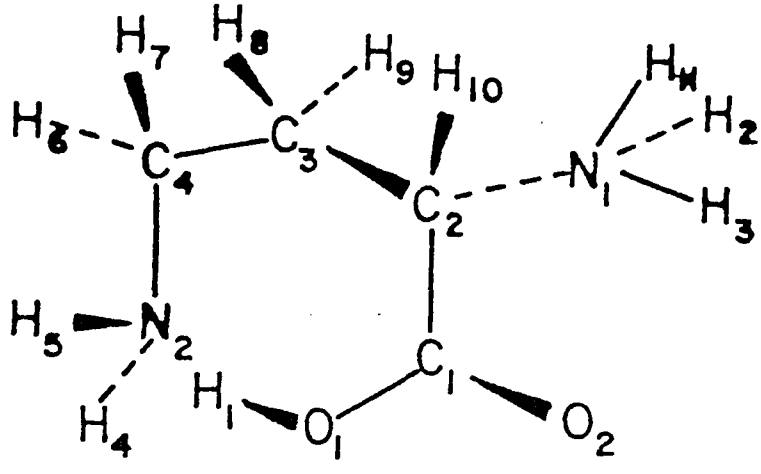

The cyclic cation of L-DABA, where protonation is at N1 and hydrogen bonding between N2 and H1.

15b

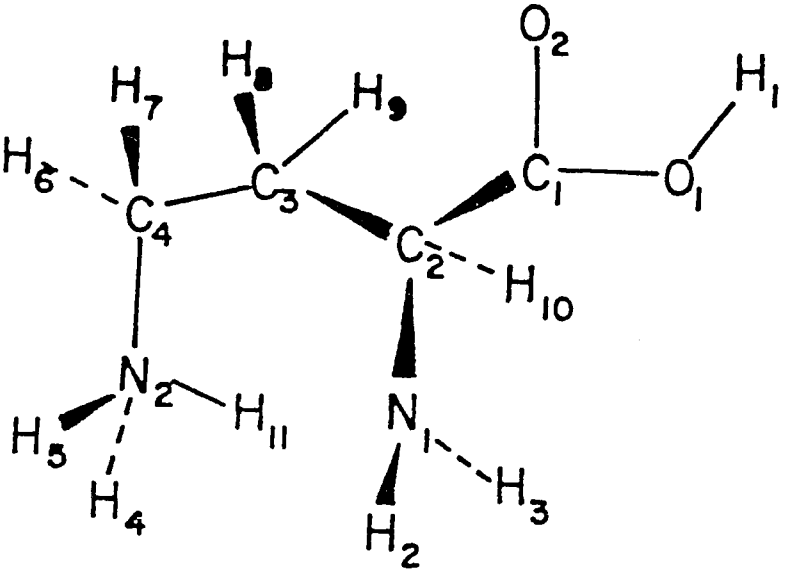

The cyclic cation of L-DABA, where protonation is at N2 and hydrogen bonding between H11 and N1.

15c

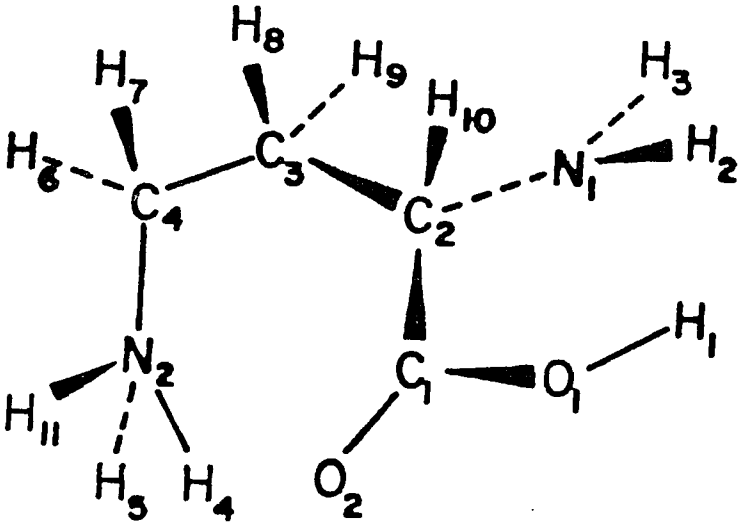

The cyclic cation of L-DABA, where protonation is at N2 and hydrogen bonding between H4 and O2.

METHODS

The method of calculation is the ab initio self-consistent field (Hartree-Fock method), as described in the methods section of Chapter 1.

The compounds in this study (1) γ-aminobutyric acid (Figure 11) partially-folded (a), cyclic (b) and extended (c); γ-aminobutyric acid imine (Figure 12) partially-folded (a) ,and cyclic (b), and (3) aminooxyacetic acid (Figure 13) partially-folded (a) and two cyclic conformations (b,c) are all geometry-optimized with the 6-31G basis set (2). In the case of GABA imine and AOAA, the extended conformations are much higher in energy and are not reported. The geometry optimization of GABA imine, (Figure 12), is performed in the following way: a number of starting geometries are used by assigning the dihedral angles C2C1N1C5, C3C2C1N1, C4C3C2C1 and O1C4C3C2 different values (for example 0°, 60°, 90°, 120°, 180°), forming a four dimensional grid. For instance, the initial geometry features one of the angles at 60°, and a number of runs are made with another angle at 90°, the third at 60° and the fourth angle at values of 60°, 90°, 120°, 180°. The procedure is repeated by setting the third angle at a different value and so on. The angles together with the other parameters of the molecule, are then allowed to relax for each value. After the optimization is performed,

the minima corresponding to Figures 12a and 12b are obtained. The starting geometries which led to the best conformations are also used as a starting geometry for GABA (Figure 11) and for AOAA (Figure 13). All the Figures mentioned above are neutral species in the gas phase. Gas phase as a model for nonpolar solvents is relevant for this study since the issue concerns transport thru the hydrophobic environment of the membrane or interaction in a non-hydrated binding site of a receptor.

The proton affinities of the neutral species for GABA and GABA imine are obtained by protonating the amino group of the most stable conformation,optimizing the geometrical parameters of the cation thus formed and subtracting the energy of the most stable conformation of the neutral species from its energy. The proton affinities of the carboxylate for GABA and GABA imine are obtained by geometry optimization of the anion and subtracting its energy from the energy of the neutral species. For AOAA, the anions investigated are those corresponding to the loss of the proton from the carboxyl of the most stable structure (which is not the most stable anion because of the repulsion of two negatively charged oxygens) and the most stable anion. The rationale is that upon proton loss from the most stable structure, the change of conformation of the anion into the most stable anionic form might go through an energy barrier. For GABA and GABA imine, the

most stable anion was the anion of the most stable neutral form.

The neutral conformations studied for L-DABA (Figure 14), in an extended (a), partially-folded (b), and cyclic (c) conformations, are all geometry-optimized with the 6-31G basis set (2).

The initial geometries are chosen as follows: in order to obtain an all-extended geometry it is sufficient to set the dihedral angles N2C4C3C2 and C4C3C2C1 at 180.0°. Several partially-folded conformations are tried and preliminary optimizations are performed. The conformation which features the dihedral angle, C4C3C2C1 of 90.0°, is found to be the most stable and is chosen for further optimization. The cyclic structure examined features a hydrogen bond between H1 and N2 (Figure 14c). In addition, calculations are performed on another cyclic structure which features a hydrogen bond between H1 and N1. This cyclic conformation is found to be much higher in energy than the cycle shown in Figure 14c and therefore it is not necessary to subject it to complete optimization. To obtain the initial cycle, leading to Figure 14c, the dihedral angles are given values which insure the formation of the H1N2 hydrogen bond. Once these structures are selected, all the parameters of the molecules, including the above mentioned dihedral angles are

allowed to relax, subject to the following constraints: for the extended and the partially-folded L-DABA, all the NH bonds, CH bonds and HCC are kept equal. For the cyclic conformation of L-DABA (where H1 is hydrogen bonded to N2), the parameters of the molecule are allowed to relax, subject to the constraint that the dihedral angle N2H1O1C1 is set at 0.0^{o}. The geometries are then optimized. After optimization is performed, the minima corresponding to Figures 14a, 14b and 14c are obtained. All the structures mentioned above are neutral species. The cyclic zwitterion of L-DABA (where N2 is protonated) is also examined by performing energy optimization.

The proton affinities of the neutral species for L-DABA are obtained by protonating each of the amino groups in turn for each conformation (extended, partially-folded and cyclic), optimizing the geometrical parameters of the cations thus formed and subtracting the energy from the most stable neutral species. The proton affinity of the carboxylate is obtained by geometry optimization of the anion and subtracting its energy from the energy of the most stable neutral species.

RESULTS

Table 7 displays the geometric parameters for GABA (Figure 11) in a partially-folded (a), cyclic (b) and extended (c) conformations. The geometric parameters for GABA imine (Figure 12) in a partially-folded (a) and cyclic (b) conformations are shown in Table 8. Table 9 displays the geometric parameters for AOAA (Figure 13) partially-folded (a) and two cyclic conformations H1 bonded to N1 (b), and H1 bonded to O1 (c). The optimized geometric parameters for L-DABA are shown in Table 10. Tables 11 and 12 display the energies for GABA, GABA imine, AOAA and L-DABA in different conformations. The total atomic charges for GABA, GABA imine, AOAA and L-DABA are shown in Tables 13, 14, 15 and 16, respectively. The proton affinities for GABA, GABA anion, GABA imine, GABA imine anion, AOAA, AOAA anion, L-DABA, and L-DABA anion are displayed in Table 17.

Table 7

Optimized bond lengths (Å), angles (degrees) for GABA (Figure 11) in a partially-folded (a), cyclic (b), and extended (c) conformations.

	11a	11b	11c
Bond lengths			
N1C1	1.454	1.475	1.472
N1H8[a]	.993	.999	.991
C1H2[b]	1.084	1.083	1.086
C2C1	1.533	1.554	1.528
C3C2	1.541	1.551	1.532
C4C3	1.496	1.512	1.494
C4O1	1.355	1.340	1.356
C4O2	1.215	1.211	1.211
O1H1	.955	.972	.955
N1H1	---	1.897	---
Bond angles			
C2C1N1	111.9	116.3	112.3
C3C2C1	113.3	118.4	111.1
C4C3C2	113.0	116.1	114.3
O1C4C3	113.3	115.9	111.3
O2C4C3	126.1	121.9	126.0
H8N1C1[c]	117.7	114.0	118.5
H2C1N1[d]	110.0	108.7	110.1
H4C2C1[e]	109.3	109.1	110.1
H1O1C4	113.5	111.1	113.6
Dihedral angles			
C3C2C1N1	61.6	22.5	180.0
C4C3C2C1	74.7	-86.7	180.0
O1C4C3C2	118.5	67.0	180.0
H9N1C1C2	91.8	-96.2	-116.9
H8N1C1C2	-125.0	136.1	111.8

a
Same bond length for N1H9.

b
Same bond length for C1H3, C2H4, C2H5, C3H6, C3H7.

c
Same bond angle for H9N1C1.

d
Same angle for H3C1N1.

e
Same angle for H5C2C1, H6C3C3, H7C3C2.

Table 8

Optimized bond lengths (Å), angles (degrees) for GABA imine (Figure 12) in a partially-folded (a) and cyclic (b) conformations.

	12a	12b
Bond lengths		
C1N1	1.458	1.462
C1H2[a]	1.084	1.083
C2C1	1.530	1.531
C3C2	1.538	1.554
C4C3	1.494	1.514
C4O1	1.355	1.340
C4O2	1.211	1.210
C5N1	1.258	1.263
C5H8	1.073	1.077
C5H9	1.083	1.083
O1H1	.955	.971
N1H1	---	1.80
Bond angles		
C1N1C5	120.9	122.7
C2C1N1	109.5	109.7
C3C2C1	111.2	113.9
C4C3C2	112.6	116.1
O1C4C3	112.3	117.2
O2C4C3	126.2	122.5
H1O1C4	113.8	116.0
***		
Dihedral angles		
C2C1N1C5	121.0	167.3
C3C2C1N1	177.1	60.6
C4C3C2C1	178.8	-96.7
O1C4C3C2	-65.1	1.40

[a] Same bond length ffor C1H3, C2H4, C2H5, C3H6, C3H7.

*** The HCC angles have been optimized together, obtaining 110.1° for 12a and 109.4° for 12b. For 12b, the H2C1N1 angle (equal to the H3C1N1 angle) has been optimized to values around 123.0°.

Table 9

Optimized bond lengths (Å), angles (degrees) for AOAA (Figure 13) partially-folded (a), cyclic where H1 is bonded to N1 (b), and another cyclic where H1 is bonded to O1 (c).

	13a	13b	13c
Bond lengths			
N1O1	1.419	1.433	1.425
N1H2[a]	.998	1.001	.999
C1O1	1.419	1.436	1.429
C1H4[b]	1.082	1.079	1.080
C2C1	1.501	1.516	1.510
O2C2	1.348	1.346	1.341
O3C2	1.210	1.205	1.205
H1O2	.955	.957	.955
N1H1	---	1.98	---
O1H1	---	---	2.0
Bond angles			
C1O1N1	116.1	114.7	112.2
C2C1O1	112.8	116.7	107.5
O2C2C1	111.1	117.3	116.2
O3C2C1	126.4	121.5	121.6
H1O2C2	114.6	115.1	114.2
H2N1O1[c]	109.9	105.7	106.5
H4C1O1[d]	109.0	106.9	110.6
Dihedral angles			
H2N1O1C1	62.2	121.5	120.0
C2C1O1N1	68.1	55.4	179.5
O2C2C1O1	167.3	-49.0	0.0

a
Same bond length for N1H3.

b
Same bond length for C1H5.

c
Same angle for H3N1O1.

d
Same angle for H5C1O1.

Table 10

Optimized bond lengths (Å), angles (degrees) for L-DABA (Figure 14) in an extended (a), partially-folded (b), and cyclic conformations (c).

	14a	14b	14c
Bond lengths			
N1C2	1.447	1.449	1.447
N1H2[a]	.994	.994	.994
N2C4	1.451	1.452	1.475
C1C2	1.509	1.512	1.530
C1O1	1.350	1.351	1.335
C1O2	1.212	1.212	1.211
C2H10	1.085	1.084	1.089
C3C2	1.539	1.540	1.556
C3H8[b]	1.085	1.084	1.084
C4C3	1.536	1.537	1.532
O1H1	.955	.955	.978
Bond angles			
N1C2C3	112.3	112.4	111.0
C1C2C3	110.1	110.9	112.3
C2C3C4	112.4	114.4	115.2
C3C4N2	114.2	113.9	112.7
H1O1C1	113.9	113.9	117.1
H2N1C2[c]	116.9	116.8	115.8
H6C4N2[d]	108.4	108.2	109.3
H8C3C4[e]	108.7	108.7	109.3
O1C1C2	112.7	112.6	116.2
O2C1C2	125.8	126.0	122.2
Dihedral angles			
C1C2C3C4	185.4	62.0	-92.9
C2C3C4N2	179.9	178.17	70.6
H1O1C1C2	181.0	180.0	---
H2N1C2C3	109.1	109.7	-111.5
H3N1C2C3	-109.1	-109.7	111.5
H4N2C4C3	73.7	68.9	86.5
H5N2C4C3	-66.3	-70.6	---
H6C4N2C3[f]	121.9	-121.9	-121.8
H7C4N2C3[g]	-121.9	121.9	121.8
H10C2C3C1	115.4	115.3	116.6
N1C2C3C1	122.8	123.4	-123.3
O1C1C2C3	64.6	58.9	55.4

a The same bond length for N1H3, N2H4, N2H5.

b
The same bond length for C3H9, C4H6, C4H7.
c
The same bond angle for H3N1C2, H4N2C4, H5N2C4.
d
The same bond angle for H7C4N2.
e
The same bond angle for H9C3C4, H10C2C3.
f
The same dihedral angle for H9C3C4C2.
g
The same dihedral angle for H8C3C4C2.

Table 11

Energies (au) for GABA (Figure 11) in a partially-folded (a), cyclic (b), extended (c) conformations, GABA imine (Figure 12) partially-folded (a), cyclic (b) conformations, AOAA (Figure 13) partially-folded (a), cyclic where H1 is bonded to N1 (b), another cyclic where H1 is bonded to O1 (c) conformations, GABA anion, GABA cation, AOAA anion and AOAA cation.

Structures	Energies	ΔE (kcal/mole)
11a	-360.7332	0
11b	-360.7253	4.95
11c	-360.7303	1.82
12a	-398.5574	0
12b	-398.5525	3.07
13a	-357.4446	3.20
13b	-357.4427	4.39
13c	-357.4497	0
GABA anion[a]	-360.1550	
GABA cation[a]	-361.0997	
GABA imine anion[b]	-397.9840	
GABA imine cation[b]	-398.9299	
AOAA anion[c]	-356.8783	
AOAA cation[c]	-357.7513	
AOAA anion[d]	-356.8917	

[a] The cation and anion of structure 11a.
[b] The anion and cation of structure 12a.
[c] The anion and cation of structure 13c.
[d] The anion of structure 13a.

Table 12

Energies for L-DABA (Figure 14) extended (a), partially-folded (b), cyclic (c) conformations and their cations and anions of these conformations.

	au	E (kcal/mole)[k]
14a	-415.7306	---
14b	-415.7296	.6[l]
14c	-415.7298	.5[m]
cation of 14a[a]	-416.0910	
cation of 14a[b]	-416.1006	
anion of 14a[c]	-415.1655	
cation of 14b[d]	-416.0905	
cation of 14b[e]	-416.1012	
anion of 14b[f]	-415.1647	
cation of 14c[g]	-416.0987	
cation of 14c[h]	-416.1163	
cation of 14c[i]	-416.1163	
anion of 14c[j]	-415.1657	

a H^+ at N1 for the extended conformation.

b H^+ at N2 for the extended conformation.

c The anion of the extended conformation.

d H^+ at N1 for the partially-folded conformation.

e H^+ at N2 for the partially-folded conformation.

f The anion of the partially-folded conformation.

g H^+ at N1 for the cyclic conformation (Figure 15a).

h H^+ at N2 for the cyclic conformation (Figure 15b).

i H^+ at N2 for the cyclic conformation (Figure 15c).

j The anion of the cyclic conformation.

k 1 atomic unit (au) is equal to 627.5 kcal/mole.

l $\Delta E = E_{\text{(Figure 14a)}} - E_{\text{(Figure 14b)}}$.

m $\Delta E = E_{\text{(Figure 14a)}} - E_{\text{(Figure 14c)}}$.

Table 13

Total atomic charges (e.u.) for GABA (Figure 11) partially-folded (a), cyclic (b) and extended (c).

	11a	11b	11c
N1	-.887	-.920	-.839
C1	-.105	-.101	-.140
C2	-.282	-.331	-.240
C3	-.387	-.413	-.411
C4	+.745	+.760	+.750
O1	-.726	-.768	+.731
O2	-.570	-.547	-.552
H1	+.434	+.506	+.436
H2	+.204	+.167	+.148
H3	+.148	+.183	+.147
H4	+.155	+.182	+.180
H5	+.165	+.186	+.182
H6	+.205	+.179	+.205
H7	+.235	+.216	+.205
H8	+.329	+.352	+.328
H9	+.339	+.347	+.329

Table 14

Total atomic charges (e.u.) for GABA imine (Figure 12) partially-folded (a), and cyclic (b) conformations.

	12a	12b
N1	-.416	-.566
C1	-.151	-.137
C2	-.298	-.328
C3	-.381	-.423
C4	+.732	+.767
C5	-.109	-.047
O1	-.728	-.777
O2	-.546	-.552
H1	+.440	+.521
H2	+.139	+.188
H3	+.188	+.181
H4	+.199	+.182
H5	+.197	+.193
H6	+.209	+.196
H7	+.202	+.217
H8	+.180	+.183
H9	+.142	+.201

Table 15

Total atomic charges (e.u.) for AOAA (Figure 13) partially-folded (a), cyclic, where H1 is bonded to N1 (b), and another cyclic where H1 is bonded to O1 (c).

	13a	13b	13c
N1	-.464	-.542	-.448
C1	-.041	-.039	-.010
C2	+.729	+.734	+.755
O1	-.533	-.564	-.664
O2	-.725	-.743	-.725
O3	-.547	-.514	-.532
H1	+.449	+.480	+.470
H2	+.370	+.367	+.355
H3	+.370	+.367	+.354
H4	+.245	+.245	+.222
H5	+.195	+.201	+.222

Table 16

Total atomic charges (e.u.) for L-DABA (Figure 14) extended (a), partially-folded (b), and cyclic (c) using 6-31G basis set

	14a	14b	14c
C1	+.747	+.750	+.777
C2	-.041	-.049	-.073
C3	-.272	-.267	-.298
C4	-.085	-.096	-.117
H1	+.442	+.442	+.530
H2	+.371	+.369	+.329
H3	+.338	+.337	+.373
H4	+.325	+.320	+.353
H5	+.321	+.323	+.353
H6	+.151	+.193	+.172
H7	+.190	+.160	+.175
H8	+.172	+.161	+.209
H9	+.162	+.168	+.170
H10	+.204	+.209	+.189
N1	-.874	-.868	-.861
N2	-.863	-.860	-.934
O1	-.730	-.732	-.789
O2	-.559	-.561	-.557

Table 17

Proton affinities of GABA, GABA anion, GABA imine, GABA imine anion, AOAA ,AOAA anion, L-DABA and L-DABA anion (kcal/mol).

GABA anion[a]	362.8	L-DABA 14a[k]	226.2
GABA[b]	230.0	L-DABA 14a[l]	232.2
GABA imine anion[c]	359.6	L-DABA 14b[m]	225.8
GABA imine[d]	234.0	L-DABA 14b[n]	232.6
AOAA anion[e]	358.6	L-DABA 14c[o]	231.0
AOAA anion[f]	350.1	L-DABA 14c[p]	242.0
AOAA[g]	189.3	L-DABA 14c[q]	242.0
L-DABA anion of 14a[h]	354.6		
L-DABA anion of 14b[i]	355.1		
L-DABA anion of 14c[j]	354.5		

a
Proton affinity (P.A.)=E (11a) - E (GABA anion)

b
P.A.=E (GABA cation) - E (11a)

c
P.A.=E (GABA imine) - E (GABA anion)

d
P.A.=E (GABA imine cation) - E (GABA imine)

e
P.A.=E (13c) - E (AOAA anion of 13c)

f
P.A.=E (13c) - E (AOAA anion of 13a)

g
P.A.=E (AOAA cation of 13c) - E (13c)

h
P.A.=E (14a) - E (anion of 14a)

i
P.A.= E (14a) - E (anion of 14b)

j
P.A.=E (14a) - E (anion of 14c)

k
P.A.=E (cation of 14a) - E (14a), [H^+ at N1]

l

P.A.=$E_{\text{(cation of 14a)}} - E_{\text{(14a)}}$, [$H^+$ at N2]

m

P.A.=$E_{\text{(cation of 14b)}} - E_{\text{(14a)}}$, [$H^+$ at N1]

n

P.A.=$E_{\text{(cation of 14b)}} - E_{\text{(14a)}}$, [$H^+$ at N2]

o

P.A.=$E_{\text{(15a)}} - E_{\text{(14a)}}$, [$H^+$ at N1]

p

P.A.=$E_{\text{(15b)}} - E_{\text{(14a)}}$, [$H^+$ at N2]

q

P.A.=$E_{\text{(15c)}} - E_{\text{(14a)}}$, [$H^+$ at N2]

DISCUSSION

As seen from Table 11, the most stable conformation for both GABA and GABA imine is a partially-folded conformation without featuring a hydrogen bond between the carboxyl hydrogen, H1 and N1. When the different starting conformations for GABA and GABA imine are allowed to relax, the most stable ones are obtained for the dihedral angles shown in Tables 7 and 8. These angles are similar to those found for GABA by Warner and Steward (82) who used CNDO/2 and also found that the partially-folded structure is the more stable conformation. However, Warner and Steward (82) used a semi-empirical method which did not optimize bond lengths and angles but assigned standard values to them. The hydrogen-bonded conformations of GABA and GABA imine (Figures 11b and 12b) represent local minima on the energy hypersurface with energies higher than Figures 11a and 12a of 4.95 kcal/mol and 3.07 kcal/mol, respectively. An all-extended structure for GABA (Figure 11c) proves to be higher in energy than Figure 11a by 1.82 kcal/mol.

When AOAA is studied, three conformations are investigated, as shown in Figures 13a-c. Figure 13c, which is found to be the most stable, features a hydrogen bond between O1 and H1. This bond has an O1H1 distance of 2.00 Å and an O2H1O1 angle of 120.0°. Next in stability, higher by 3.20 kcal/mol is the partially-folded

conformation (Figure 13a), similar to the most stable structure of GABA. Less stable than Figure 13c by 4.39 kcal/mol is Figure 13b which features a hydrogen bond between N1 and H1. The net atomic charges for AOAA on N1 and O1 in Figure 13a (Table 15) are -.464 e.u. and -.533 e.u. respectively. Since O1 is more negative than N1 it attracts H1 more. Upon O1-H1 bond formation, O1 increases its negative charge (by .131 e.u.) to -.664 e.u. When N1 forms a bond with H1 its negative charge increases by only .078 e.u. Thus, it can be assumed that AOAA penetrates the BBB because it has a cyclic hydrogen-bonded structure which might be more lipophilic than the structure obtained for GABA. An argument in favor of this hypothesis is that a compound also found to cross the blood-brain barrier is 5-fluoro-pentanoic acid, a potent inhibitor of GABA transaminase, in which there is probably a hydrogen bond between the carboxyl hydrogen and the fluorine in the 5 position (66).

It is clear that, in water, many other conformations of GABA, and the GABA zwitterion may be present. However, in the gas phase, the energy of the zwitterion in a cyclic form, obtained by setting H1 on N1 instead of O1 and optimizing the other parameters of the molecule, is higher by approximately 20 kcal/mol than the neutral species.

As seen in Table 12, the extended, partially-folded

and cyclic structures for L-DABA are almost equal in energy, the extended (Figure 14a) being the lowest in energy. Next, lowest in stability to the extended is the cyclic conformation where H1 and N2 are hydrogen-bonded and the H1N2 distance is 1.7 Å (Figure 14c), with .5 kcal/mole more energy. The partially-folded conformation for L-DABA, which does not feature a hydrogen bond is next in stability, higher by .6 kcal/mole than the extended. The population percentage is 55.9% for the extended, 24.3% for the cyclic and 19.8% for the partially-folded. Other partially-folded conformations for L-DABA are also examined. Preliminary calculations on one partially-folded conformation, where the dihedral angle C1C2C3C4 is 80°, C1C2C3N2 is 181°, O1C1C2C3 is 3.0° and H1O1C1O2 is set at 0.0°; is found to be higher in energy (10 kcal/mol) than the partially-folded structure reported in Figure 14b. Therefore, the partially-folded structure reported is the most stable partially-folded neutral species. Since all three conformations for L-DABA (the extended, partially-folded and cyclic) are so close in energy, it is likely that they may all coexist in vivo. Furthermore, in a hydrated environment in vivo, the zwitterion may the most stable. In the gas phase however, it is found that the energy of the zwitterion in a cyclic form, (obtained by setting H1 on N2 instead of O1), is

higher in energy than the neutral species by 25 kcal/mol. When Table 16 is examined one notices that in the cyclic form, Figure 14c, C1 is more positive than it is for the other conformations while O1 bears a larger negative charge than for the conformations depicted in Figures 14a and 14b. The increased positive charge on H1 in Figure 14c is typical for a hydrogen bond.

An important factor which has bearing on the lipophilicity and perhaps on the ability to cross the BBB is the proton affinities of the amino groups and the carboxyl group. A higher proton affinity at NH_2 facilitates the formation of the NH_3^+ group, while a low proton affinity of the carboxylate leads to the formation of the anion. The carboxyl group proton affinities for GABA, GABA imine and AOAA are quite similar (Table 17). However, the proton affinities of the NH_2 group in GABA and AOAA are quite different. The proton affinity of the amino group of AOAA is lower than the proton affinities of the amino group of GABA and of the imino group of GABA imine (Table 17). Therefore, GABA and GABA imine are expected to exist as cations in polar solvents and be solvated in water. AOAA will be less protonated, less hydrated and cross the BBB.

The most stable cations for L-DABA are the cyclic forms where H^+ is positioned on N2 (Figures 15b and 15c, Table 18). The hydrogen-bonded cyclic structures (Figures 15b and 15c) had the same energy. In the case of GABA, a

cation similar to Figure 15c is shown to be 7.3 kcal/mol more stable than the cation of the partially-folded GABA. The cations for L-DABA which had H^+ positioned on N2 are found to be more stable than the cations which had H^+ positioned on N1 for the partially-folded, extended and cyclic conformations. Upon examining the proton affinities of L-DABA, one sees that the highest proton affinity for L-DABA is higher than GABA (242 versus 237.3 kcal/mol). The carboxyl group proton affinity for GABA (362.8 kcal/mol), is higher than for L-DABA (354 kcal/mol) in all the conformations examined (the extended, partially-folded and cyclic), which is consistent with the presence of the α-amino group in L-DABA. The high proton affinity of the N2-amino group of L-DABA and the low proton affinity of its anion suggest a low lipophilicity for L-DABA and therefore it is probable that diffusion alone cannot account for the barrier crossing.

L-DABA has been suggested to cross the BBB, while GABA does not (4,77). It can be inferred from the examination of compounds which do cross the BBB for example AOAA and 5-fluoro-4-amino-pentanoic acid, that the presence of a neutral cyclic structure may facilitate this transport (64,67). GABA and GABA imine has been shown in this study to have a higher energy in a cyclic noncharged conformation (where H1 and N1 are hydrogen bonded) than in a partially-folded conformation, while L-DABA fea-

tures an uncharged cyclic structure almost as stable as the extended and the partially-folded conformation. Since in vivo studies suggest that L-DABA does cross the BBB, this process may involve mediated transport of DABA.

It has been shown in several studies that L-DABA strongly inhibits high-affinity GABA uptake in synaptosomal tissue (73-76). Moreover, Debler and Lajtha showed that L-DABA inhibits (89%) high-affinity GABA uptake in synaptosomal (P2) tissue (79). It has been suggested that the synaptosomal binding sites for GABA are specific and recognize L-DABA. This study suggest that L-DABA inhibits high-affinity synaptosomal uptake because of its apparent flexibility. It can be seen (Table 12) that the different conformations of L-DABA exhibit almost the same energies and therefore it would be relatively easy for L-DABA to adopt a conformation complementary to a GABA binding site. The conformational flexibility of L-DABA probably accounts for its inhibition of taurine uptake (23%) as well as glycine uptake (27%), (79).

As shown by Erecinska and coworkers, GABA is co-transported by a high-affinity carrier in synaptosomal tissue with two Na^+ and DABA with one Na^+ (46,47). This observation is compatible with the fact that the proton affinity of DABA is 4.5 kcal/mol higher than GABA. Therefore at neutral pH, DABA is cationic (+1) and GABA is neutral.

Chapter 3. *Ab initio* calculations on taurine and hypotaurine.

INTRODUCTION

Taurine (2-aminoethanesulphonic acid, $^{+}NH_3CH_2CH_2SO_3^{-}$) is found widely distributed in nature, from algae to mammals (85). In mammals, taurine is found in high concentrations in brain, retina, myocardium, liver and muscle as well as in platelets, lymphocytes and cerebrospinal fluid (86,87).

Taurine biosynthesis involves several pathways [Figure 16, (86)].

Figure 16

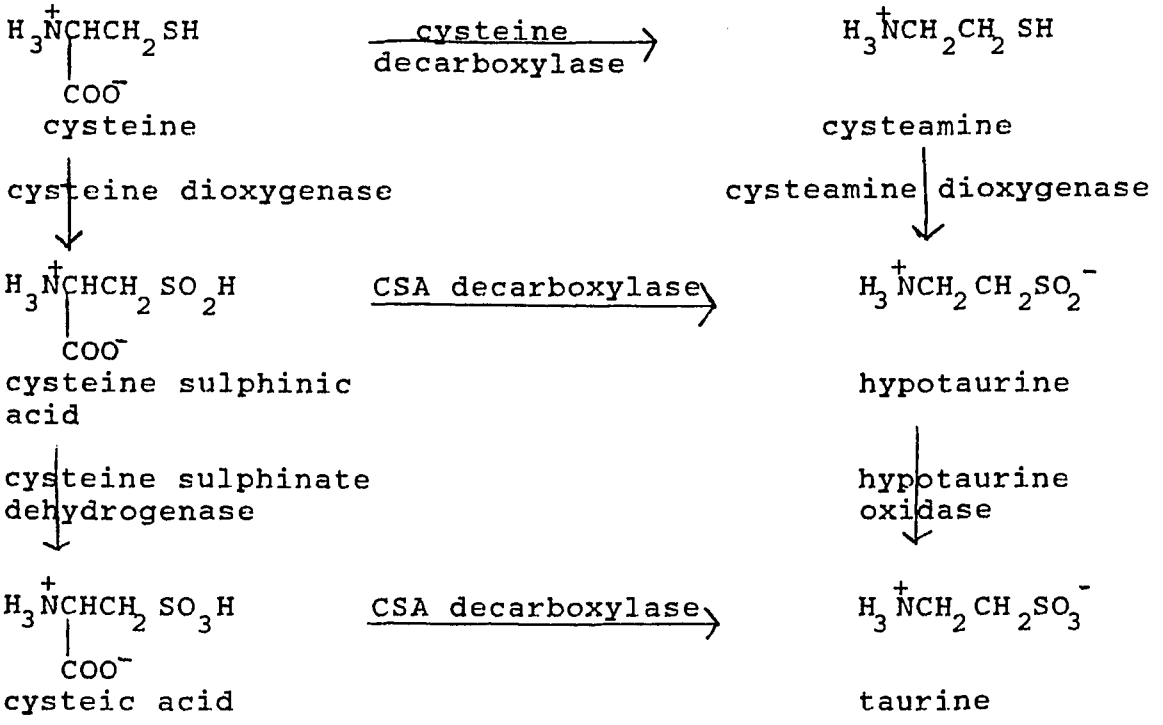

The first pathway, called the CSA (cysteine sulfinic acid) pathway, involves the conversion of cysteine to cysteine sulfinic acid catalyzed by cysteine dioxygenase. Cysteine sulfinic acid is oxidized to cysteic acid by cysteine sulfinate dehydrogenase. Cysteic acid is then decarboxylated to the final product taurine by the action of the enzyme cysteine sulfinic acid decarboxylase (CSAD), (88). In the second pathway, called the cysteamine pathway, cysteine is converted to cysteamine by cysteine decarboxylase, which is oxidized to hypotaurine by hypotaurine oxidase and finally to taurine.

The third pathway, which is the major route for taurine biosynthesis in the brain is the decarboxylation of cysteine sulfinic acid to hypotaurine by CSAD, and oxidation of hypotaurine to taurine (88).

Taurine has been shown to be an important amino acid in retinal function (89-91). Hayes and coworkers (89) showed that severe retinal changes and blindness developed in cats fed a taurine-deficient diet. Another study reported that taurine-depleted cats developed a disorganization of their retinal tapetum (92). Studies on primates have shown similar results, in that, monkeys on taurine-free diets developed visual acuity-loss associated with morphological changes in photoreceptors (90,91). Moreover, it was shown in one study that children receiving taurine-free, long term total parenteral nutrition,

had decreased taurine concentrations in the plasma which resulted in abnormalities in the electroretinogram, that was correctible with taurine administration (93,94). Taurine has been postulated to have several functions in the eye (86). Taurine may regulate osmotic pressure and retinal Ca^{2+} homeostasis and it inhibits the phosphorylation of specific retinal membrane proteins. Taurine stabilizes retinal membranes and it has also been implicated in scavenging hypochlorous acid generated by peroxidase present in retinal-pigmented epithelial cells.

Bile salts are important for digestion and absorption. Bile salts act on the surface of emulsified lipid droplets containing triglycerides and increase their water solubility (85). Moreover, bile salts promote the action of a lipase contained in human milk which can promote the hydrolysis of triglycerides even in the absence of pancreatic lipase. Bile acids are conjugated with either taurine or glycine before their secretion in bile. Studies on rats and in guinea pigs showed that taurine prevented cholestasis (a condition in which bile acids and cholesterol levels are elevated), induced by the secondary bile acid, lithocholate sulfate, or by its glycoconjugate (95,96). Another study showed, that when hamsters were fed taurine, the rate of bile flow increased and the activity of cholesterol-7-α-hydroxylase was stimulated (97,98). Because cholesterol- 7-α-hydroxylase is the rate-

limiting step in the conversion of cholesterol to bile acids, the protective effect of taurine against cholesterol gallstone formation has been attributed to this mechanism (99,100).

Taurine functions as an osmotic regulator of cell size in sharks, fishes, rats and marine bacteria (85). The levels of taurine are regulated by specific Na^+-dependent active transport processes that are responsive to changes in osmolality and composition of the extracellular fluid. Changes in plasma osmolalities are accompanied by corresponding changes in the content of intracellular taurine, which help to maintain a constant cell size. Taurine has also been implicated in the stabilization of membranes in skeletal muscle and heart muscle (86).

Some investigators have suggested that taurine is an inhibitory neurotransmitter (101). Taurinergic neurons are a distinct synaptosomal population because CSAD has been located in a synaptic population and synaptic vesicles containing taurine are also present in mammalian cerebral cortex (102-104). It was observed that taurine caused depression of neuronal firing of single neurons of the cerebral cortex, spinal cord and medulla (105,106). Alterations in the concentration of taurine in the brain may be of importance with respect to the pathology of epilepsy (107). Taurine administered peripherally to mice or cats with cobalt-induced epilepsy, produced anticonvulsant

action (106-110).

The transport of taurine has been extensively studied. High-affinity and low affinity transport processes have been identified (79,101,111-114). It has been postulated by Hanretta and Lombardini (101) that one possible function of the high-affinity uptake system is to remove extracellular synaptic taurine, released by taurinergic neuronal activity, in order to limit the duration of the action of taurine on postsynaptic receptor sites. The low affinity uptake of taurine functions to remove taurine (released by glial and neuronal cells) that diffuses away from the synaptic cleft, thus working in concert with the neuronal high-affinity uptake system to remove extracellular taurine from the synaptic area in order to preserve the integrity of information relayed through the taurinergic synapse (101). Larsson and colleagues demonstrated high-affinity uptake systems for GABA, taurine and β-alanine in cultured neurons and astrocytes (49). Taurine and β-alanine exhibited reciprocal inhibition of uptake and probably use a carrier different from GABA. In addition, Debler and Lajtha (79) showed the existence of three separate high-affinity transport systems for the uptake of GABA, taurine and glycine respectively, in cortical synaptosomal tissue. Lahdesmaki and Oja found that hypotaurine and β-alanine are potent inhibitors of taurine uptake in rat brain slices (115). High-affinity

taurine uptake in rat brain has been shown to be Na^+-dependent (100,111-114,116). Borg and coworkers reported that two Na^+ ions were co-transported with one taurine molecule in both neuronal and glial cells in culture (116). Another study using whole brain rat synaptosomes, also reported two Na^+ ions were cotransported with one taurine (113). While, Hanretta and coworkers (101) reported one Na^+ ion was co-transported with each taurine molecule in rat hypothalamic crude P2 synaptosomes. The differences in the number of Na^+ ions cotransported may be attributed to regional or cellular differences. A low-affinity uptake process identified in rat hypothalamic synaptosomes was also found to be Na^+-dependent (101).

Franconi and his colleagues compared taurine and several analogs for their action on tension in guinea pig ventricular strips (117). Taurine-like activity had a strict requirement for two carbon atoms between the sulfonic and amino groups. This observation might lead to information about the size of the binding site on a taurine receptor. Also in this study, it was noted that when the aliphatic chain was replaced with an aromatic ring, activity was still present only when the sulfonic and amino groups were bound to adjacent carbons on the ring. A possible explanation is that taurine binds in a planar conformation which defines the geometry of receptor-taurine interaction for this activity (117).

Experimental results show taurine to cross the BBB very slowly, while the more lipophilic pivaloyltaurine does so readily (105,118). As mentioned in Chapter 2 GABA has been shown not to penetrate the BBB (4). The ability of hypotaurine to penetrate the BBB has not been reported in the literature. The conformational structure of taurine and hypotaurine may influence their ability to penetrate the BBB. This study uses ab initio calculations to elucidate the conformation and charge distribution of taurine and hypotaurine in the gas phase, a medium which simulates the non-hydrated environment of the inner membrane leaflet. The structural characteristics of taurine and hypotaurine are compared to GABA, in order to identify similarities and differences between their lowest energy conformations and correlate those findings with the ability of these compounds to cross the BBB. Their ability to inhibit each other and other amino acids in high-affinity transport on synaptosomal tissue, is also correlated with their structures. The compounds studied are taurine (Figure 17) in an extended (a), partially-folded (b) and two cyclic conformations, where H1 is hydrogen-bonded to N1 (c), and H2 is hydrogen-bonded to O2 (d), and the cyclic cation of taurine (e). Hypotaurine (Figure 18), the precursor to taurine, in an extended (a), partially-folded (b), and cyclic (c) conformations and the cyclic cation (d) are examined. The anion of taurine in an extended

conformation and partially-folded cation and anion of hypotaurine are also studied.

17a

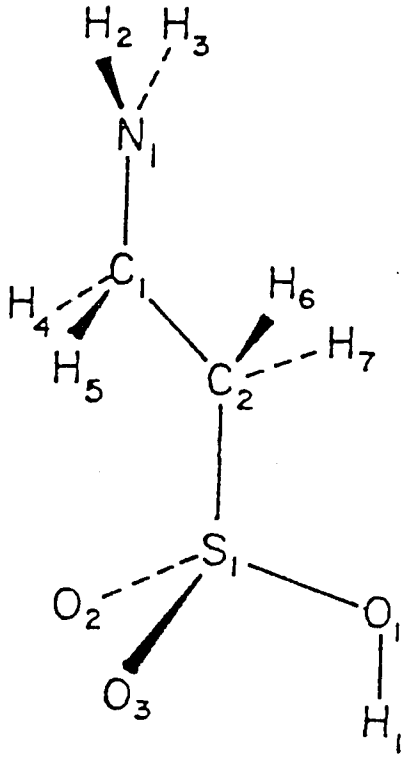

Taurine in an extended conformation.

17 b

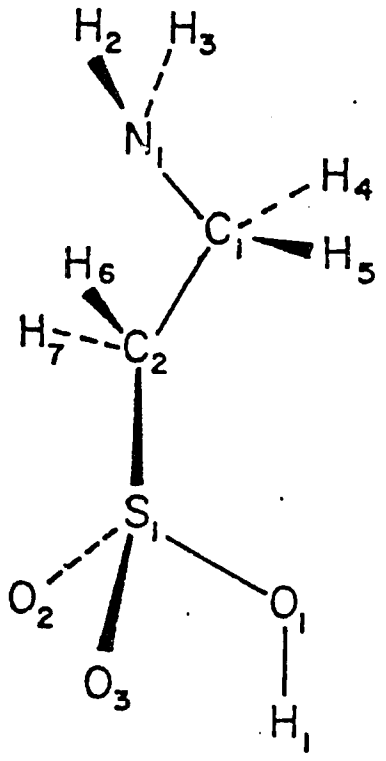

Taurine in a partially-folded conformation.

17c

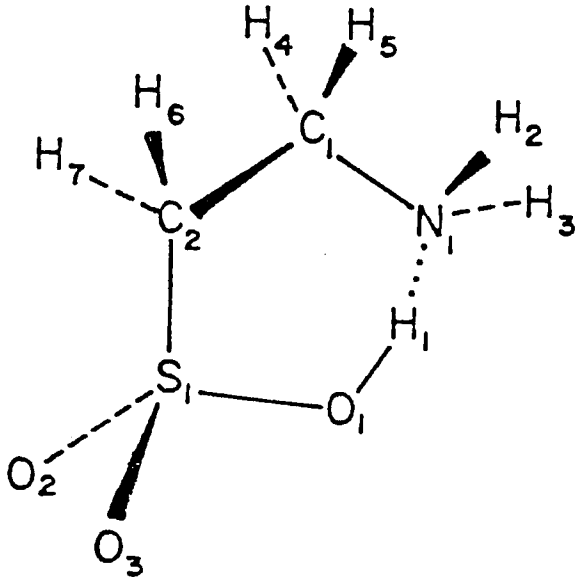

Taurine in a cyclic conformation, where H1 is bonded to N1.

17d

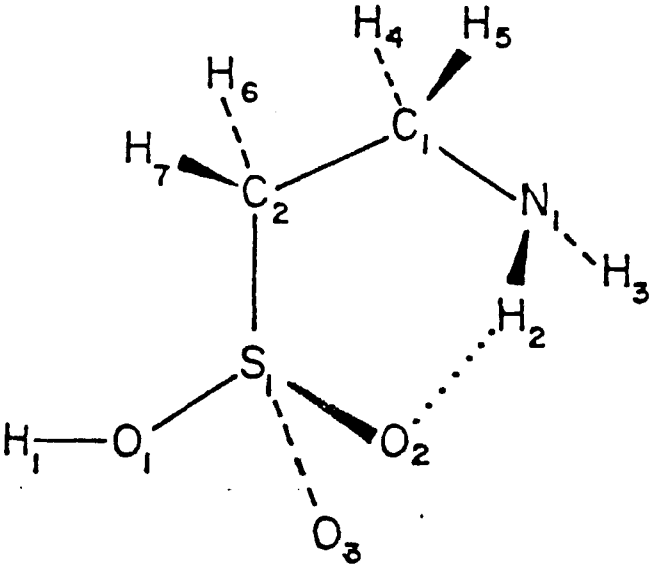

Taurine in a cyclic conformation, where O2 is bonded to H2.

17e

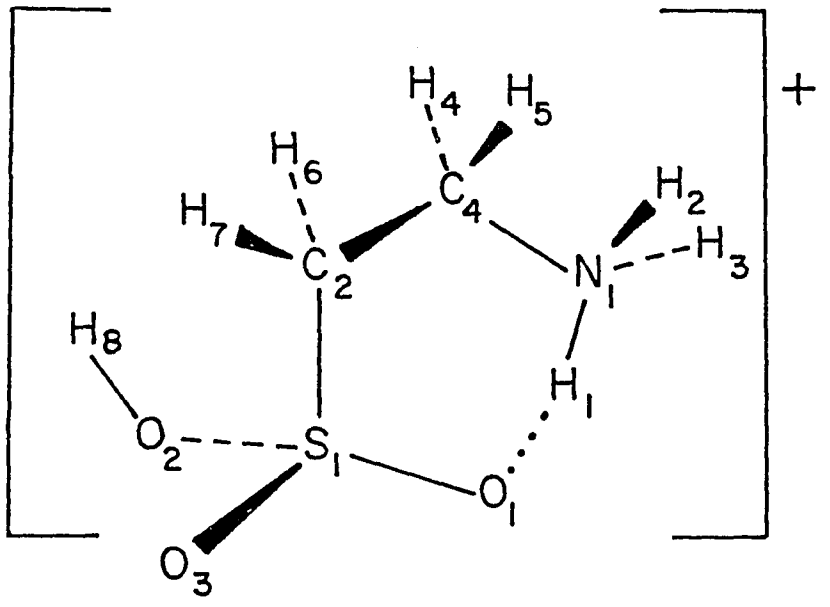

The cyclic cation of taurine.

18a

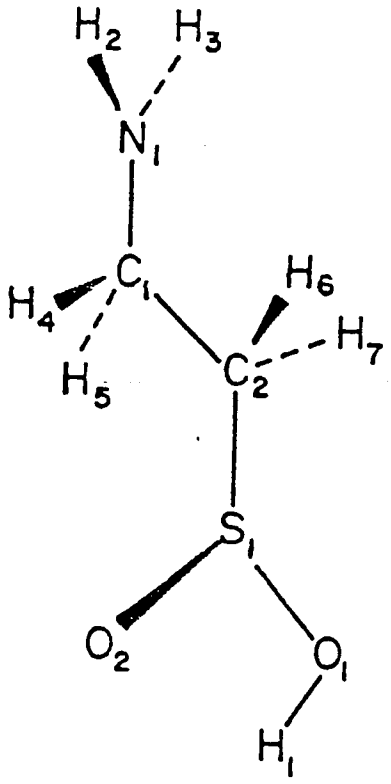

Hypotaurine in an extended conformation.

18b

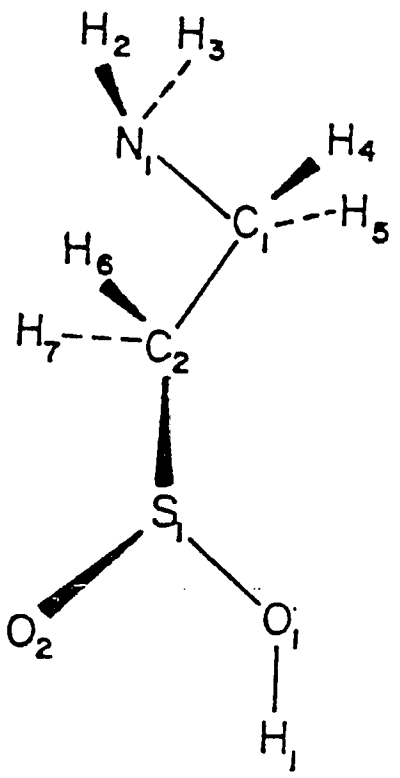

Hypotaurine in a partially-folded conformation.

18 c

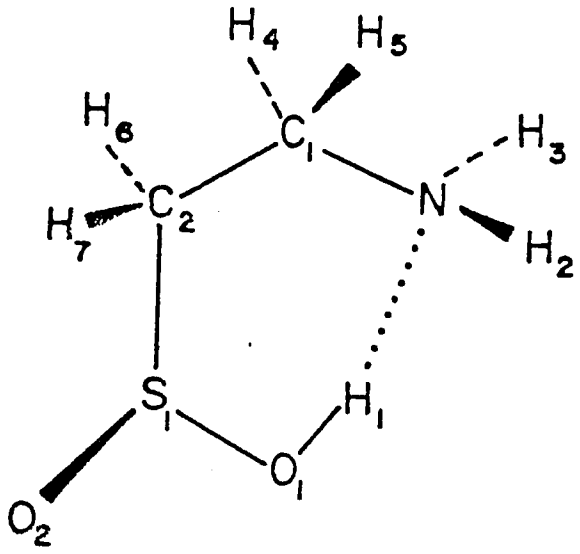

Hypotaurine in a cyclic conformation.

18d

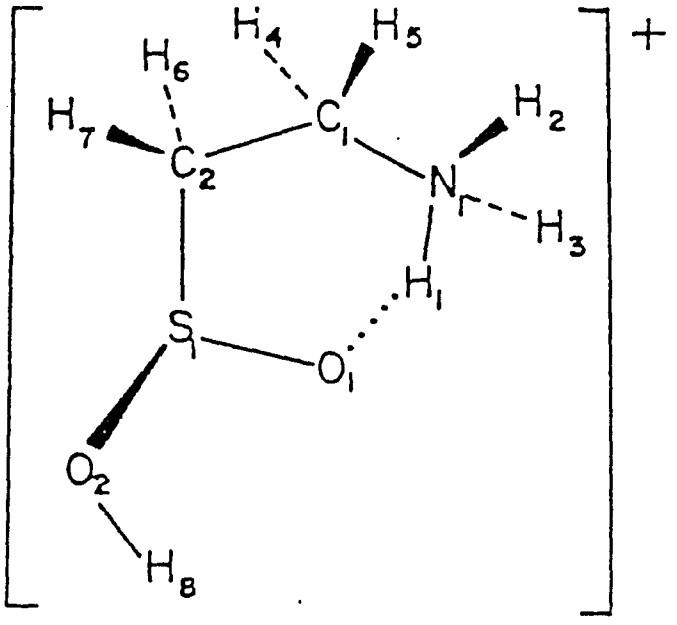

The cyclic cation of hypotaurine.

METHODS

The energies of taurine and hypotaurine in different conformations (extended, partially-folded and cyclic) are calculated using quantum chemical methods. The method of calculation is the ab initio (Hartree-Fock) method as described in the Methods section of Chapter 1.
The compounds in this study, (1) taurine (Figure 17) extended (a), partially-folded (b) and cyclic (c) conformations and (2) hypotaurine (Figure 18) in extended (a), partially-folded (b) and cyclic (c) conformations are all geometry-optimized with the 6-31G basis set (2). The optimized geometries are also used to obtain single-point energies and charges using the 6-31G* basis set, which is known to be more reliable in this respect especially for sulfur containing compounds. (119).

Several starting geometries (extended, partially-folded and cyclic conformations) are studied.
For each starting geometry, the parameters of the molecule are allowed to relax, subject to the following constraints: all the NH bonds, the CH bonds, the HCC angles and the HNC angles are kept equal. The OSC angles and the SO bonds between the sulfur and oxygen atoms, which do not have a hydrogen positioned on them, are kept equal. The geometry is then optimized. To obtain the starting geometries, the dihedral angle between the N1C1C2 plane and the C1C2S1 plane takes the initial

values: 40° for the cyclic structures, 90° for the partially-folded structure and 180° for the extended structure. Optimization around these values allows the system to relax in each local minimum, covering in this way, all the possible intermediate conformations.

When the cyclic structures are considered, the rotation of the SO1 and NH2 bonds are performed initially so as to obtain Figures 17c and 17d. For each of these the dihedral angle, O1S1C2C1, is allowed to relax.

For the initial geometry for the extended conformation of taurine, the dihedral angles C1C2S1O1 and H1O1S1C2 are given the value 180.0° and H2N1C1C2 is given the value 60.0°. The dihedral angles and the other parameters of the molecule are then allowed to relax for each value. After optimization is performed, the minimum corresponding to Figure 17a is obtained. For the partially-folded and cyclic conformations of taurine, the dihedral angles are also given initial values and then allowed to relax for each value, together with the other parameters of the molecule. After optimization is performed, the minima corresponding to Figures 17b and 17c are obtained.

For the initial geometry of the extended conformation of hypotaurine, the dihedral angles C1C2S1O1 and H1O1S1O2 are given the value 180.0° and H2N1C1C2 is given the value 60.0°. The dihedral angles and the other parameters of the molecule are then allowed to relax for each value. The

minimum corresponding to Figure 18a is obtained after optimization. Dihedral angles and other parameters of the molecule for the partially-folded and cyclic conformations of hypotaurine, are assigned different values chosen in the same way as for taurine and then allowed to relax for each value. Preliminary calculations had shown that the C2 is not in the plane of the SO2 group. The minima corresponding to Figures 18b and 18c are obtained after optimization is performed. The zwitterion of taurine is also examined, performing optimization.

These calculations identify the most stable conformations in the gas phase and possibly these are the conformations which have to be considered when predicting if a molecule can diffuse across the membrane i.e. the blood-brain barrier.

The proton affinities of taurine and hypotaurine are calculated as the difference between the most stable cation and its most stable neutral species. Another cation, shown in Figure 18d is also examined. The proton affinity of the anion is calculated as the difference between the most stable neutral species and the most stable anion.

RESULTS

Figures 17 and 18 display the compounds being investigated. Table 18 shows the optimized geometries for the extended and cyclic conformation of taurine using 6-31G. Table 19 displays optimized geometries for the extended, partially-folded and cyclic conformation of hypotaurine. The energies for taurine and hypotaurine in the extended, partially-folded and cyclic conformations and the energies of the cations and anions are shown in Table 20. Table 21 displays the total atomic charges for the cyclic conformation of taurine (Figure 17c) which is the most stable conformation, and the total atomic charges for the most stable conformation of hypotaurine which is the partially-folded one (Figure 18b). The proton affinities for taurine and hypotaurine and their anions are shown in Table 22.

Table 18

Optimized bond lengths (Å), angles (degrees) for taurine (Figure 17) extended (a) and cyclic (c) conformations using 6-31G basis set.

	17a	17c
Bond lengths		
C1C2	1.545	1.528
C1N1	1.438	1.474
C1H4[a]	1.078	1.079
H2N1[b]	0.991	0.998
N1H1	---	2.101
O1H1	0.960	0.970
S1C2	1.851	1.853
S1O1	1.704	1.699
S1O2[c]	1.640	1.642
Bond angles		
C1C2S1	108.9	108.5
C2S1O1	101.7	103.2
C2S1O2[d]	108.4	107.0
H1O1S1	114.1	108.0
H2N1C1[e]	119.6	114.3
H4C1C2[f]	109.5	108.8
H6C2S1[g]	105.9	105.1
N1C1C2	110.2	110.8
Dihedral angles		
C1C2S1O1	180.0	78.9
H1O1S1C2	180.0	190.6
H2N1C1C2	78.1	114.8
H3N1C1C2	-78.1	-114.8
C2C1N1H1	---	-6.2
S1C2C1N1	180.0	68.0

a
Same bond length for C1H5, C2H6, C2H7.
b
Same bond length for H3N1.
c
Same bond length for S1O3.
d
Same bond angle for C2S1O3.
e
Same bond angle for H3N1C1.

f
 Same bond angle for H5C1C2.
g
 Same bond angle for H7C2S1.

Table 19

Optimized bond lengths (Å), angles (degrees) for hypotaurine (Figure 18) extended (a), partially-folded (b) and cyclic (c) using 6-31G basis set.

	18a	18b	18c
Bond lengths			
C1C2	1.537	1.528	1.531
C1H4[a]	1.080	1.080	1.080
C1N1	1.443	1.456	1.475
N1H1	---	---	2.105
N1H2[b]	.991	.993	.997
O1H1	.961	.960	.964
S1C2	1.860	1.861	1.860
S1O1	1.739	1.743	1.738
S1O2	1.673	1.670	1.665
Bond angles			
C1C2S1	109.8	110.8	111.2
C2S1O1	97.7	96.8	96.8
C2S1O2	102.4	102.9	102.6
H1O1S1	110.0	109.9	108.0
H2N1C1[c]	119.3	117.6	115.2
H4C1C2[d]	109.8	108.8	109.3
H6C2S1[e]	106.2	105.0	105.4
N1C1C2	111.8	111.4	111.9
Dihedral angles			
C1C2S1O1	182.2	61.7	80.5
H1O1S1O2	-0.6	0.7	---
H2N1C1C2	76.5	108.6	114.1
H3N1C1C2	-76.5	-108.6	-114.1
N1C1C2S1	179.3	61.8	---
O2S1C2O1	105.9	104.9	108.1

a Same bond length for C1H5, C2H6, C2H7.

b Same bond length for N1H3.

c Same bond angle for H3N1C2.

d Same bond angle for H5C1C2.

e Same bond angle for H7C2S1.

Table 20

Energies for taurine (Figure 17) extended (a), partially-folded (b), cyclic (c) conformations and for the best cation and anion conformation, and for hypotaurine (Figure 18) extended (a), partially-folded (b), cyclic (c) and the best conformation of the cation and anion using 6-31G and 6-31G*.

	6-31G		6-31G*	
	au	ΔE (kcal/mole)[d]	au	ΔE (kcal/mole)[d]
17a	-755.9162	+2.4[e]	-756.1703	+7.0[e]
17b	-755.9088	+7.1[f]	---	---
17c	-755.9201	0	-756.1813	0
18a	-681.1959	+1.3[g]	-681.3692	+1.2[g]
18b	-681.1979	0	-681.3711	0
18c	-681.1909	+4.4[h]	-681.3688	+1.4[h]
taurine cation	-756.2741[a]		-756.5300	
taurine anion	-755.3988[b]		-755.6600	
hypotaurine cation	-681.5787[c]		---	
hypotaurine anion	-680.6246[c]		-680.7914	

a The cation of 17c.

b The anion of 17a.

c The cation and anion of 18b.

d 1 atomic unit (au) is equal to 627.5 kcal/mole.

e $\Delta E = E_{(1c)} - E_{(1a)}$

f

$$\Delta E = E_{(17c)} - E_{(17b)}$$

g

$$\Delta E = E_{(18b)} - E_{(18a)}$$

h

$$\Delta E = E_{(18b)} - E_{(18c)}$$

Table 21

Total atomic charges (e.u.) for the cyclic conformation of taurine (Figure 17c) and for the partially-folded conformation of hypotaurine (Figure 18b) calculated using 6-31G*.

	17c	18b
C1	-.143	-.136
C2	-.552	-.546
H1	.522	.480
H2	.395	.341
H3	.373	.334
H4	.230	.185
H5	.196	.222
H6	.261	.238
H7	.238	.213
N1	-.954	-.865
O1	-.801	-.833
O2	-.677	-.782
O3	-.719	---
S1	1.631	1.150

Table 22

Proton affinities (kcal/mol) using the most stable conformations of taurine anion, taurine, hypotaurine anion, hypotaurine, GABA anion, GABA, AOAA anion and AOAA calculated using 6-31G and 6-31G*.

	6-31G	6-31G*
taurine anion[a]	324.7	320.2
taurine[b]	222.1	218.8
hypotaurine anion[c]	359.7	355.0
hypotaurine[d]	238.9	239.3
GABA anion[e]	362.8	---
GABA[e]	230.0	---
AOAA anion[e]	358.6	---
AOAA[e]	189.3	---

[a] Proton affinity (P.A.) = $E_{(17c)} - E_{(\text{anion of } 17a)}$

[b] P.A. = $E_{(17e)} - E_{(17c)}$

[c] P.A. = $E_{(18b)} - E_{(\text{anion of } 18b)}$

[d] P.A. = $E_{(\text{cation of } 18b)} - E_{(18b)}$

[e] Data taken from Chapter 2.

DISCUSSION

As seen from Tables 18 and 20, the most stable conformation for taurine is the cyclic conformation (Figure 17c) which features a hydrogen bond between the hydrogen of the sulphonic acid group and the nitrogen. This result is in agreement with the conclusions of Franconi and coworkers (117) and with Liebowitz and Lombardini (120) who suggest a gauche conformation around C1C2 for taurine (117,120). Indeed, a gauche conformation can feature a hydrogen bond between the hydrogen of the sulphonic group and the nitrogen. A conformation (Figure 17d) featuring a hydrogen bond between the amino hydrogen and O2 was found to be high in energy and therefore is not discussed. Next in stability for taurine is the extended form (Figure 17a), which is higher in energy than the cyclic form by only 3 kcal/mol. Thus both are very likely to coexist in vivo. In fact, in a hydrated environment in vivo, the zwitterion may be the most stable. The partially-folded conformation studied (Figure 17b) is higher than the cyclic conformation (Figure 17c) by 7 kcal/mol. This might be influenced by the fact that the partially-folded conformation which does not feature hydrogen bonding, brings the oxygens too close to the nitrogen, introducing an electrostatic repulsion. The most stable cation for taurine is shown in Figure 17e, where the oxygen (O1) in the sulphonic group is hydrogen-bonded to a charged NH_3^+

group, while a proton is positioned on O2.

In hypotaurine, since the third oxygen is absent, the nitrogen can position itself close to the sulfur as shown in Figure 18b, which is the most stable conformation examined. Next in stability for hypotaurine is the extended conformation (Figure 18a), higher in energy by only 1 kcal/mol, which is not significant. The hydrogen-bonded conformation, which features a hydrogen bond between the nitrogen and the hydrogen of the sulphinic group (18c) is not as stable as 18a and 18b. It is higher in energy than 18b by 4 kcal/mol. The most stable cation of hypotaurine is formed by adding a proton to the NH_2 group in Figure 18b. The other cation depicted in Figure 18d is found to be higher in energy.

The geometries of the extended and cyclic forms of taurine do not show major differences in bond lengths and angles. The same holds true for hypotaurine. For taurine and hypotaurine, one notices an elongation of the C1N1 bond for the cyclic conformations. The N1H1 distance in the cyclic forms of taurine and hypotaurine is 2.1 Å, which is the upper limit of hydrogen bond lengths.

As mentioned taurine is known to cross the BBB slowly, while GABA does not cross the BBB at all (4,103). The presence of a neutral cyclic structure in most cases, is the most lipophilic and a cycle seems to increase the lipo-

philicity and therefore would increase the ability of different compounds to cross the BBB. GABA has been shown in previous results not to adopt a cyclic form while amino-oxyacetic acid (AOAA) which crosses the BBB, is cyclic and neutral in its stable conformation. An important factor which has bearing on lipophilicity, are the proton affinities of the amino groups and in this case of the sulfonic and sulfinic group. When the charged species are examined it is found that among the cations, the most stable cation for taurine is the cyclic one shown in Figure 17e. Examining the proton affinity of taurine one sees that it is much lower than the proton affinities of GABA and GABA imine by 8.3 kcal/mol. This fact would favor its crossing the BBB by increasing its lipophilicity. However, at the 6-31G level the proton affinity of the sulphonate group is 38 kcal/mol less than that of the carboxyl group, a factor which decreases its lipophilicity. Due to the hydrogen bonding between the sulphonic hydrogen and the amino nitrogen in the cyclic structure of taurine, the amino group can not be protonated. But while taurine can assume a cyclic noncharged conformation to traverse the hydrophobic region of the membrane, in the aqueous compartment it may be charged and solvated appreciably. This would account for its crossing the BBB slowly.

An attempt to transfer the sulphonic hydrogen to the nitrogen leading to the formation of a cyclic zwitterion,

showed the cyclic zwitterion to be higher in energy than the neutral species by 8 kcal/mole. It is found that the cyclic zwitterion represents a true minimum. The NH distance corresponding to this minimum is 1.08 Å. As the N1H1 increases, the energy increases also, showing the presence of a barrier to the proton transfer from the amino group to the sulphonic group. However, when the hydrogen becomes bound to the sulphonic group the energy is lower.

Because the most stable form for hypotaurine is not the cyclic and its proton affinity is similar to that of GABA, it may be inferred that hypotaurine will not cross the BBB. No charge-based arguments can be provided, since the charges in taurine and hypotaurine, are quite similar except that O1 and O2 are more negative in hypotaurine because of the absence of O3. The total charges of the amino groups are very similar.

Previous work by Debler and Lajtha (79) suggests that the synaptosomal binding sites for GABA are specific and recognize L-DABA (2,4-diaminobutyric acid) (89% inhibition) and hypotaurine (56% inhibition). This might be related to the similar partially-folded conformations of GABA and hypotaurine. Results on DABA show that it also features a partially-folded conformation, which is as stable as the extended and cyclic conformations.

Synaptosomal uptake of taurine is inhibited by a ten-

fold molar excess of β-alanine and hypotaurine (93 and 103% inhibition respectively) and less well by the same concentrations of GABA and proline [58 and 49% inhibition respectively (79)].

It is tempting to hypothesize that the unhydrated structures and conformations are best recognized by the receptor binding sites. In such a case, a partially-folded conformation for GABA, DABA and hypotaurine would fit in the GABA binding site. In the taurine-receptor interaction, the decisive factor may be related to the distance between the amino group and the acid groups. Indeed, it is found that the distance between the nitrogen and the farthest oxygen (which is not bound to hydrogen) to be very similar for taurine and hypotaurine in their most stable conformations (4.57 and 4.69 Å, respectively).

References

1. Hehre, W.J., Stewart, R.F. and Pople, J.A. (1969) Self-consistent molecular-orbital methods. Use of Gaussian expansions of Slater-type atomic orbitals. J. Chem. Phys. 51, 2657-2664.

2. Hehre, W.J., Ditchfield, R. and Pople, J.A. (1972) Self-consistent molecular orbital methods. Further extensions of Gaussian-type basis sets for use in molecular orbital studies of organic molecules. J. Chem. Phys. 56, 2256-2261.

3. Ford, G.C., Eichele, G. and Jansonius, J. (1980) Three dimensional structure of a pyridoxal-phosphate dependent enzyme, mitochondrial aspartate aminotransferase. PNAS 77, 2259-2563.

4. Krogsgaard-Larsen, P. (1981) γ-aminobutyric acid agonist, antagonist and uptake inhibitors. Design and therapeutic aspects. J. Med. Chem. 24, 1377-1383.

5. Tagaki, W. and Westheimer, F. (1968) Acetoacetate decarboxylase. Reassociation of subunits. Biochemistry 7, 891-901.

6. Porthsmouth, D., Stoolmiller, A. and Abeles, R. (1967) Studies on the mechanism of action of 2-keto-3-deoxy-L-arabonate dehydratase. J. Biol. Chem. 242, 2751-2759.

7. Tavan, P, Schulten, K. and Oesterchelt, D. (1985) The effectof protonation and electrical interactions on the stereochemistry of retinal Schiff bases. J. Biophys. 47, 415-430.

8. Honig, B. and Ebrey, T. (1974) The structure and spectra of the chromophore of the visual pigments. Ann. Rev. Biophys. Bioenerg. 3, 151-177.

9. Oseroff, R. and Callender, R.H. (1974) Resonance Raman spectroscopy of rhodopsin in retinal. Biochem. 13, 4243-4248.

10. Ottolenghi, M. (1980) The photochemistry of rhodopsin. Adv. Photochem. 12, 97-200.

11. Birge, R.R. (1981) Photophysics of light transduction in rhodopsin and bacteriorhodopsin. Ann. Rev. Biophys. Bioenerg. 10, 315-354.

12. Bridges, C.D.B. (1967) Spectroscopic properties of porphyrosins. Vision Res. 7, 349-369.

13. Hubbard, R. and Kropf, A. (1967) Molecular isomers in vision. Sci. Am. 216, 64-76.

14. Hubbard, R. (1969) Absorption spectrum of rhodopsin: 500 nm absorption band. Nature 221, 432-435.

15. Honig, B., Denur, V., Nakanishi, K., Balogh-Nair, V., Gawinowicz, M.A., Arnaboldi, M. and Motto, M.G. (1979) An external point-charge model for wavelength regulation in visual pigments. J. Am. Chem. 101, 7084-7086.

16. Nakanishi, K., Balogh-Nair, V., Arnaboldi, M., Tsujimoto, K. and Honig, B. (1980) An external point-charge model for bacteriorhodopsin to account for its purple color. J. Am. Chem. Soc. 102, 7945-7947.

17. Oesterhelt, D. and Stroechenius, W. (1971) Rhodopsin-like protein from the purple membrane of Halobacterium Halobium. Nature [New Biol.] 233, 149-152.

18. Walker, J.E., Carne, A.F. and Schmitt, H. (1979) The topography of the purple membrane. Nature 278, 653-654.

19. Lozier, R.H., Bogomolni, R.A. and Stoechenius, W. (1975) Bacteriorhodopsin: a light-driven proton pump in Halobacterium halobium. Biophys. J. 15, 955-967.

20. Favrot, J., Leclerq, J.M., Roberge, R., Sandorfy, R., Sandorfy, C. and Vocelle, D. (1979) Intermolecular interactions in visual pigments. The hydrogen bond in vision. Photochem. Photobiol. 29, 99-108.

21. Zuccarello, F., Raudino, A. and Buemi, G. (1984) Environment effect on the shape of the absorption band of rhodopsin. J. Mol. Struct. (THEOCHEM) 107, 215-220.

22. Raudino, A., Zuccarello, F. and Buemi, G. (1984) Spectral properties of rhodopsin. J. Chem. Soc. Faraday Trans. 79, 1750-1754.

23. Hodošček, M. and Hadži, D. (1985) Ab initio calculations on the retinal Schiff base-formic acid and allylimine-formic acid hydrogen bonds. Can. J. Chem. 63, 1528-1531.

24. Sapse, A.M. and Russell, C.S. (1986) Theoretical studies of the binding of methylamine and guanidine to carboxylate. J. Mol. Struct. (THEOCHEM) 137, 43-53.

25. Sapse, A.M. and Russell, C.S. (1984) Ab initio calculations of guanidinium-carboxylate interaction. Int. J. Quant. Chem. 26, 91-99.

26. Bray, D.D., Slattery, N. and Russell, C.S. (1984) Guanidinium-carboxylate interaction: methylguanidinium formate. Int. J. Peptide Protein Res. 24, 414-418.

27. Binkley, J.S., Whiteside, R.A., Kirshman, R., Seiger, R., DeFries, D.J., Schlegel, H.B.; Topiol, S. Kahn, L.R. and Pople, J.A. (1980) Gaussian-80, Depart. of Chem., Carnegie Mellon Univ., Pittsburg P.A., 15213.

28. Schlegel, H.B. (1984) Optimization, equilbrium geometries and transition structures. J. Comput. Chem. 3, 214-218.

29. Del Bene, J.E., Worth, G.T., Marchese, F.T. and Conrad, M.E. (1975) Ab initio molecular orbital study of substituted carbonyl compounds. Theo. Chim. Acta 36, 195-206.

30. Gersten, J.I., Sapse, A.M. (1985) Generalization of the Born equation to nonspherical solvent cavities. J. Am. Chem. Soc. 107, 3786-3788.

31. Bissonnette, M. and Vocelle, D. (1984) Interactions of carboxylic acids with all-trans-retinylidene-tert-butylamine. Chem. Phys. Lett. 111, 506-510.

32. Bissonnette, M., Thanh, H.L. and Vocelle, L.D. (1985) Etudie d'un modele simplifie de la rhodopsin: la toute trans-retinylidene-tert-butylamine en presence de divers acides carboxyliques. Can. J. Chem. 63, 1480-1486.

33. Jain, D., Sapse, A.M. and Coburn, D. (1988) Solvent effect on some imine-carboxyl complexes. J. Phys. Chem. 92, 6847-6849.

34. Schade J.P. and Ford D.H. (1973) Basic Neurology. Elsevier, New York, pp 78-80.

35. McGeer, P.L., Eccles, J.C. and McGeer, E.G. (1978) Molecular Neurobiology of the Mammalian Brain. Plenum Press, New York, pp 144-149.

36. Cooper, J.B., Bloom, F.E. and Roth, R.H. (1982) The biochemical basics of Neuropharmacology. Oxford University Press, New York, pp 249-294.

37. Turner, A.J. and Whittle, S.R. (1983) Biochemical dissection of the γ-aminobutyric acid synapse. Biochemistry 209, 29-41..

38. Baxter, C.F.(1976) GABA in Nervous system function. Raven Press, pp 61-88.

39. Tapia, R. and Covarrubias, M. (1978) Amino acids as chemical transmitters. Plenum Press, pp 431-438.

40. Sze, P.Y. (1979) GABA biochemistry and CNS functions (Adv. Exp. Biol., vol. 123), Plenum Press, 59-78.

41. Maitre, M., Ossola, L.and Mandel, P. (1979) GABA-biochemistry and CNS functions (Adv. Exp. Med. Biol. vol. 123), Plenum Press, pp 3-20.

42. Krogsgaard-Larsen (1980) Inhibitors of the GABA uptake systems. Molecular and Cellular Biochem. 32, 105-121.

43. Schousboe, A., Larsson, O.M., Wood, J.D. and Krogsgaard-Larsen, P. (1983) Transport and metabolism of γ-aminobutyric acid in neurons and glial : implications for epilepsy. Epilepsia 24, 531-537.

44. Schon, F. and Kelly, J.S. (1975) The characterization of [^{3}H] GABA uptake into the satellite glial cells of rat sensory ganglia. Brain Res. 86, 243-257.

45. Larsson, O.M., Drejar, J., Hertz, L. and Schousboe, A. (1983) Ion dependency of uptake and release of GABA and (RS)-nipecotic acid studied in cultured mouse cortex neurons. J. Neurosci. Res. 9, 291-302.

46. Erecinska, M. (1987) The neurotransmitter amino acid transport systems. Biochem. Pharm. 36, 3547-3555.

47. Erecinska, M., Troegar, M. and Alston, T.A. (1986) Amino acid neurotransmitters in the CNS. Properties of L-2,4-diaminobutyric acid transport. J. Neurochem. 46, 1452-1457.

48. Seiler, N. and Lajtha, A. (1987) Neurotrophic activity of GABA during development. Alan Liss Inc., pp 1-56.

49. Larsson, O.M., Griffiths, R., Allen, I.C. and Schousboe, A. (1986) Mutual inhibition kinetic analysis of γ-amino-butyric acid, taurine and β-alanine high-affinity transport into neurons and astrocytes: evidence for similarity between the taurine and β-alanine. J. Neurochem. 47, 426-432.

50. Yu, A. and Hertz, L. (1982) Uptake of glutamate, GABA and glutamine into a predominantly GABA-ergic and a predominantly glutamatergic nerve cell population in culture. J. Neurosci. Res. 7, 23-35.

51. Schousboe, A. (1979) GABA biochemistry and CNS function. Plenum Press, pp 219-237.

52. Martin, D.L. (1987) Carrier-mediated transport and removal of GABA from synaptic regions. Raven Press, pp. 1-56.

53. Meldrum, B.S., Croucher, M.J. and Krogsgaard-Larsen, P. (1982) Problems in GABA research from brain to bacteria, Excerpta Medica, pp 182-91.

54. Meldrum, B.S. (1975) Epilepsy and γ-aminobutyric acid mediated inhibition. Int. Rev. Neurobiol. 17, 1-36.

55. Bakay, R.A.E. and Harris, A.B. (1981) Neurotransmitter, receptor and biochemical changes in monkey cortical epileptic foci. Brain Res. 206, 387-404.

56. Ribak, C.E., Harris, A.B., Vaughn, J.E. and Roberts, E. (1979) Inhibitory GABAergic nerve terminals decrease at sites of focal epilepsy. Sci. 205, 211-214.

57. Ross, S.M. and Craig, C.R. (1981) Studies on γ-amino-butyric acid transport in cobalt experimental epilepsy in the rat. J. Neurochem. 36, 1006-1011.

58. Christensen, A.V. and Krogsgaard-Larsen, P. (1984) Neurotransmitters, seizures and epilepsy. Raven Press, pp 109-126.

59. Bird, E.D. and Iverson, L.L. (1974) Huntington's chorea: postmortem acetyltransferase and dopamine in basal ganglia. Brain Res. 97, 457-472.

60. Perry, J.L., Hansen, S. and Kloster, M. (1973) Huntington's chorea, deficiency of γ-aminobutyric acid in brain. N. Engl. J. Med. 288, 337-345.

61. Urguhart, N., Perry, T.L., Hansen, S. and Kennedy, J. (1975) GABA content and glutamic acid decarboxylase activity in brain of Huntington's chorea patients and control subjects. J. Neurochem. 24, 1071-1075.

62. Yunger, L.M., Fowler, P.J., Zarevics, P. and Setler, P.S. (1984) Novel inhibitors of GABA uptake: anti-convulsant actions in rats and mice. J. Pharmacol. Exp. Ther. 228, 109-115.

63. Lajtha, A. (1962) Handbook of Neurochemistry, 2nd edition, Plenum Press, pp 399-430.

64. Nishibori, M., Oishi, R., Itoh, Y. and Saeki, K. (1986) Effects of GABA-mimetic drugs on turnover of histamine in the mouse brain. Japan. J. Pharmacol. 41, 403-408.

65. Lipert, B., Metcalf, B.W., Jung, M.J. and Cassara, P. (1977) 4-amino-hex-5-enoic acid a selective catalytic inhibitor of 4-aminobutyric acid aminotransferase in mammalian brain. Eur. J. Biochem. 74, 441-445.

66. Silverman, R.B., Invergo, B.J. and Mathew, J. (1986) Inactivation of -aminobutyric acid aminotransferase by (S.E.) -4-amino-5-fluoropent-2-enoic acid and effect on the enzyme of (E)-3-(1-aminocyclopropyl)-2-propenoic acid . J. Med. Chem. 29, 1840-1846.

67. Silverman, R.B. and Invergo, B.J. (1986) Mechanism of inactivation of γ-aminobutyrate aminotransferase by 4-amino-5-fluoropentanoic acid. First example of an enamine mechanism for a γ-aminoacid with a partition ratio of 0. Biochem. 25, 6817-6820.

68. Cubells, J.F., Blanchard, J.S. and Makman, M.H. (1987) The effects of *in vivo* inactivation of GABA transaminase and glutamic acid decarboxylase on levels of GABA in the rat retina. Brain Res. 419, 208-215.

69. Schechter, P.J., Hanke, N.F., Grove, J., Huebert, N. and Sjoerdsma, A. (1984) Biochemical and clinical effects of γ-vinyl-GABA in patients with epilepsy. Neurology 34, 182-186.

70. Malizia, L.A. and Tunnicliff, G. (1987) Uptake of γ-aminobutyric acid by catfish brain. J. Biochem. Physiol. 87c, 37-40.

71. Tunnicliff, G. and Ngo, T.T. (1982) Competitive inhibition of γ-aminobutyric acid synaptosomal uptake by ABBA. J. Neurochem. 39, 998-1000.

72. Sutton, I. and Simmonds, M.A. (1974) The selective blockade by DABA of neuronal uptake of [^{3}H] GABA in rat brain in vivo. J. Neurochem. 23, 273-274.

73. Iverson, L.L. and Kelly, J.S. (1975) Uptake and metabolism of γ-aminobutyric acid by neurones and glial cells. Biochem. Pharmacol, 24, 933-938.

74. Simon, J.R. and Martin, D.L. (1973) Effects of L-2,4-aminobutyric acid on the uptake of γ-aminobutyric acid by synaptosomal fraction of rat brain. Archiv. Biochem. Biophys. 157, 348-355.

75. Weitsch-Dick, F., Jessell, T.M. and Kelly, J.S. (1978) The selective neuronal uptake and release of [^{3}H] DL-2,4-diaminobutyric acid by rat cerebral cortex. J. Neurochem. 30, 799-806.

76. Simon, J.R., Martin, D.L. and Kroll, M. (1974) Sodium dependent efflux and exchange of GABA in synaptosomes. J. Neurochem. 23, 981-991.

77. Chen, C.H., Flory, W. and Koeppe, R.E. (1972) Variation of neurotoxicity of L-and D-2,4-diaminobutyric acid with route of administration . Tox. Appl. Pharmol. 23, 334-338.

78. Horton, R.W., Collins, J.F., Anlezark, G.M. and Meldrum, B.S. (1979) Convulsant and anticonvulsant actions in DBA/2 mice of compounds blocking the re-uptake of GABA. Eur. J. Pharmol. 59, 75-83.

79. Debler, E.A. and Lajtha, A. (1987) High-affinity transport of γ-aminobutyric acid, glycine, taurine, L-aspartic acid and L-glutamic acid in synaptosomal (P2) tissue: a kinetic and substrate specificity analysis. J. Neurochem. 48, 1851-1856.

80. Pullman, B. and Berthod, H. (1975) Molecular orbital studies on the conformation of γ-aminobutyric acid. Isolated molecule and solvent effect. Theoret. Chim. Acta (Berl) 36, 317-328.

81. Kier, L.B. and Truitt, E.B. (1970) Molecular orbital studies on the conformation of GABA and muscimol. Experimentia 26, 988.

82. Warner, D. and Steward, E.G. (1975) CNDO-2 molecular orbital calculations on the conformation modes of GABA. J. of Mol. Struct. 25, 403-411.

83. Goldstein, G.W. and Betz A.L. (1974) The blood-brain barrier. Sci. Am. 255, 74-83.

84. Anderews, P.R., Iskander, M.N., Jones, G.P. and Winkler, D.A. (1982) Design of transition-state analogues for GABA-transaminase. J. Quantum Chem. 9, 345-353.

85. Chesney (1985) Taurine: its biological role and clinical implications. Adv. Ped. 32, 2-42.

86. Wright, C.E., Tallan, H.H. and Lin, Y.Y. (1986) Taurine: its biological update. Ann. Rev. Biochem. 55, 427-453.

87. Gaull, G.E. (1982) Taurine in the nutrition of the human infant. Acta Paediatr. Scang. (Suppl.) 296, 38-40.

88. Jacobsen, J.G. and Smith, L.H. (1968) Biochemistry and physiology of taurine and taurine derivatives. Physiol. Rev. 48, 424-511.

89. Hayes, K.C., Carey, R.E. and Schmidt, S.Y. (1975) Retinal degeneration associated with taurine deficiency in the cat. Sci. 188, 950-951.

90. Imaki, H., Moretz, R., Wiseniewski, H., Neuringer, M. and Sturman, J. (1987) Retinal degeneration in 3-month-old rhesus monkey infants fed a taurine free human infant formula. J. Neurosci. Res. 18, 602-605.

91. Neuringer, M. and Sturman, J. (1987) Visual acuity-loss in rhesus monkey infants fed a taurine-free human infant formula. J. Neurosci. Res. 18, 597-601.

92. Wen, G.Y., Sturman, J.A. and Wisniewski, H.M. (1979) Tapetum disorganization in taurine depleted cats. Invest. Opthalmol. Vis. Sci. 18, 1201-1209.

93. Geggel, H.S., Ament, M.E. and Heclenlively, J.R. (1985) Nutritional requirements for taurine in patients receiving long-term parenteral nutrition. N. Eng. J. Med. 312, 142-146.

94. Vinton, N.E., Laidlaw, S.A., Ament, M.E. and Kopple, J.D. (1987) Taurine concentration in plasma, blood cells and urine of children undergoing long term parenteral nutrition. Ped. Res. 21, 399-403.

95. Yousef, I.M., Tuchweber, B. and Vonk, R.J. (1981) Lithocholate cholestasis: sulfated glycolithocholate induced intrahepatic cholestasis. Gastroent. 80, 233-241.

96. Dorvil, N.P., Yousef, I.M. and Tuchweber, B. (1983) Taurine prevents cholestasis induced by lithocholic sulfate in guinea pigs. Am. J. Clin. Nutr. 37, 221-223.

97. Bellantani, S., Pecovari, M.I., Cordoma, P. , Marchegiano, P., Manenti, F. (1987) Taurine increases bile acid pool size and reduces bile saturation index in the hamster. J. Lipid Res. 28, 1021-1027.

98. Nakamura-Yamanaka, Y., Tsuji, K. and Ichikawa, T. (1987) Effect of dietary taurine on cholestero-7-alpha-hydroxylase activity in the liver of mice fed a lithogenic diet. J. Nutri. Sci. Vitaminol. 33, 239-243.

99. Hepner, G.W. and Quarfordt, S.H. (1975) Kinetics of cholesterol and bile acid in patients with cholesterol cholelithiasis. Gastroent. 69, 318-325.

100. Fujihara, E., Kaneta, S. and Ohshima, T. (1978) Strain difference in mouse cholelithiasis and the effect of taurine on the gallstone formation in C57BL/C mice. Biochem. Med. 19, 211-217.

101. Hanretta, A.T. and Lombardini, J.B. (1987) Is taurine a hypothalamic neurotransmitter? A model of differential uptake and compartmentalization of taurine by neuronal and glial cell particles from the rat hypothalamus. Brain Res. Rev. 12, 167-201.

102. DeBelleroche, J.S. and Bradford, H.F. (1977) Amino acids in synaptic vesicles from mammalian cerebral cortex. J. Neurochem. 21, 441-451.

103. Karasawa, N., Yoshida, M. , Sakai, M., Teramura, M. and Nagatsu, I. (1989) Immunohistocytochemical studies of taurine- and GABA-like immunoreactive structures in rat cerebellum. Biogenic amines 6, 233-240.

104. Kassin, D.E., Sturman, J.A. and Gaull, G.E. (1977) Taurine in developing rat brain: subcellular distribution and association with synaptic vesciles of ^{35}S taurine in maternal, fetal, and neonatal rat brain. J. Neurochem. 28, 41-50.

105. Oja, S., Kontro, P., Linden, I.B. and Gothoni, G. (1983) Anticonvulsant activity of some 2-aminoethanesulphonic acid (taurine) derivatives. Eur. J. Pharmacol. 87, 191-198.

106. Van Gelder, N.M. (1983) A central mechanism of action for taurine: osmoregulation, bivalent cations and excitation threshold. Neurochem. Res. 8, 687-690.

107. Van Gelder, N.M. (1972) Antagonism by taurine of cobalt-induced epilepsy in cat and mouse. Brain Res. 47, 157-165.

108. Izumi, K.H., Igisu, H. and Fukada, T. (1974) Suppression of seizures by taurine-specific or nonspecfic. Brain Res. 76, 171-175.

109. Kontro, P. and Oja, S.S. (1987) Effects of the anticonvulsant taurine derivative, taltrimide, on membrane transport and binding of GABA and taurine in the mouse cerebrum. Neuropharmacol. 26, 19-23.

110. Fariello, R.G., Golden, G.T. and Ente, P. (1986) The epileptogenic action of TAG: nonspecific versus specific antitaurine pathogenesis. Brain Res. 380, 196-200.

111. Hruska, R.E., Thut, P.D., Huxtable, R. and Bressler, R. (1976) Taurine. Raven, N.Y. pp 347-356.

112. Hruska, R.E., Padjin, A., Bressler, R. and Yamamura, H.I. (1978) Taurine, sodium-dependent, high-affinity transport into rat brain synaptosomes. Mol. Pharmacol. 14, 77-85.

113. Kontro, P. and Oja, S.S. (1978) Sodium dependence of taurine uptake in rat brain synaptosomes. Neurosci. 3, 761-765.

114. Holopainen, I., Malminen, O. and Kontro, P. (1987) Sodium-dependent high-affinity uptake of taurine in cultured cerebellar granule cells and astrocytes. J. Neurosci. Res. 18, 479-483.

115. Lahdesmaki, P. and Oja, S.S. (1973) On the mechanism of taurine transport and brain cell membranes. J. Neurochem. 20, 1411-1417.

116. Borg, J., Balcar, V.J., Mark, J. and Mandel, P. (1979) Characterization of taurine uptake by neuronal and glial cells in culture. J. Neurochem. 32, 1801-1805.

117. Franconi, F., Failli, P., Stendardi, I., Matucci, R., Bernardini, F., Baccarro, C., Giotta, A. (1986) Positive inotropic effect of some taurine-related compounds on guinea-pig ventricular strip perfused with low calcium medium. Eur. J. Pharmacol. 124, 129-133.

118. Ahtee, L., Auvinen, H., Maenpaa, A.R., Vahala, M.L., Lehtinen, M.M. and Halmk, J. (1985) Comparison of central nervous actions of taurine and N-pivaloyl-taurine. J. Acta Pharmacol. et Tox. 57, 96-105.

119. Szabo, A. and Ostlun, N.S. (1982) Modern Quantum Chemistry. Macmillan, New York, pp 189-192.

120. Liebowitz, S.M., Lombardini, J.B. and Salva, P. (1987) Cyclic taurine analogs: synthesis and effects on ATP-dependent Ca uptake in rat retina. Biochem. Pharm. 36, 2109-2114.